

Relativistic heavy-ion physics: three lectures

L. McLerran

Brookhaven National Laboratory, Upton, NY 11973, USA and RIKEN BNL Research Center,
Brookhaven National Laboratory, Upton, NY 11973, USA

Abstract

These lectures provide an introduction to the physics issues which are being studied in the collisions of ultrarelativistic heavy ions. The lectures are focused on the production of new states of matter. The quark–gluon plasma is thermal matter which once existed in the Big Bang. The colour glass condensate is a universal form of high energy density gluonic matter which is part of a hadron wavefunction and which controls the high-energy limit of strong interactions. The glasma is matter produced in the collisions of high-energy hadrons which evolves into a quark–gluon plasma. The glasma has interesting topological properties and may be responsible for the early thermalization seen at RHIC. I introduce the student to these topics, discuss results from experiments, and comment upon future opportunities.

1 Introduction

These lectures will introduce the student to the physics issues behind the study of new forms of matter, and the general issue of understanding the high-energy limit of QCD. The full programme of this study involves the collisions of protons on protons, deuterons on nuclei, nuclei on nuclei, and electrons on protons and nuclei. The reason for using nuclei is that one can achieve extraordinary energy densities of matter, and, because of the large size of nuclei relative to partons, more easily study effects associated with the bulk properties of matter. The highest energies are required, as this allows one to generate the highest energy densities, and as we shall see, at RHIC energies and higher, one can study novel effects associated with the high density of gluons in a hadron wavefunction.

Central to these experimental studies is the production of new forms of matter. This may be a Quark–Gluon Plasma (QGP) or a Colour Glass Condensate (CGC). The properties of these forms of matter are described below.

The outline of these lectures is

– **New states of matter**

In the first lecture, I describe the new forms of matter which may be produced in heavy-ion collisions. These are the quark–gluon plasma, the colour glass condensate, and the glasma.

– **Space–time dynamics**

This lecture describes the space–time dynamics of high-energy heavy-ion collisions. In this lecture, I illustrate how high energy density matter might be formed. I describe how the colour glass condensate may produce a glasma which evolves into the quark–gluon plasma, and eventually to a gas of ordinary hadrons.

– **Experiment and theory**

In the final lecture, I show how various experimental measurements might teach us about the properties of matter. Topics discussed are multiplicities and the colour glass condensate, low-transverse-momentum particles and the quark–gluon plasma, heavy vector meson production and confinement, the flavour dependence of the quark–gluon plasma, high-transverse-momentum particles and what they tell us about the CGC and the QGP, and identical particle correlations and what they tell us about the space–time evolution of the matter produced in collisions.

2 Lecture I: High-density matter

2.1 The goals of RHIC

The goal of nuclear physics has traditionally been to study matter at densities of the order of those in the atomic nucleus

$$\epsilon \sim 0.15 \text{ GeV/fm}^3 . \quad (1)$$

High-energy nuclear physics has extended this study to energy densities several orders of magnitude higher. This extension includes the study of matter inside ordinary strongly interacting particles, such as the proton and the neutron, and producing new forms of matter at much higher energy densities in high-energy collisions of nuclei with nuclei, and various other probes.

There are at least three central issues of high-energy nuclear physics:

- **The properties of matter close to thermal equilibrium at energy densities greater than one or two orders that of nuclear matter**

This matter is at such high densities that it is only simply described in terms of quarks and gluons and is generically referred to as the Quark–Gluon Plasma (QGP). The study of this matter may allow us to better understand the origin of the masses of ordinary particles such as nucleons, and of the confinement of quarks and gluons into hadrons. The QGP will be described below [1].

- **The study of the matter which controls high-energy strong interactions**

This matter is believed to be universal (independent of the hadron), and exists over sizes large compared to the typical microphysics size scales important for high-energy strong interactions. (The microphysics size scale here is about 1 fm and the microphysics time scale is the time it takes light to fly 1 fm, $t \sim 10^{-23}$ s.) The matter appears in the wavefunctions of a hadron, and is called a Colour Glass Condensate (CGC) because it is composed of coloured particles, evolves on time scales long compared to microphysics time scales and therefore has properties similar to glasses, and a condensate since the phase-space density of gluons is very high. In collisions, this matter forms a glasma, which eventually evolves into a quark–gluon plasma, for hadrons of large enough size (for example, nuclei). The study of these forms of matter may allow us to better understand the typical features of strong interactions when they are truly strong, a problem which has eluded a basic understanding since strong interactions were first discovered. The CGC and the glasma will be described below [2].

- **The study of the structure of the proton, most notably spin**

The structure of the proton and neutron is important as these particles form the ordinary matter from which we are composed. We would like to understand how valence quantum numbers such as baryon number, charge, and spin are distributed. RHIC has an active programme to study the spin of the proton [3].

Because I was asked to provide lectures on ultrarelativistic nuclear collisions, I shall discuss only the first two issues.

2.2 The quark–gluon plasma

This section describes the quark–gluon plasma, why it is important for astrophysics and cosmology, and why it provides a laboratory in which one can study the origin of mass and of confinement [1].

2.2.1 What is the quark–gluon plasma?

Matter at low energy densities is composed of electrons, protons, and neutrons. If we heat the system, we might produce thermal excitations which include light-mass strongly interacting particles such as the pion. Inside the protons, neutrons, and other strongly interacting particles are quarks and gluons. If we

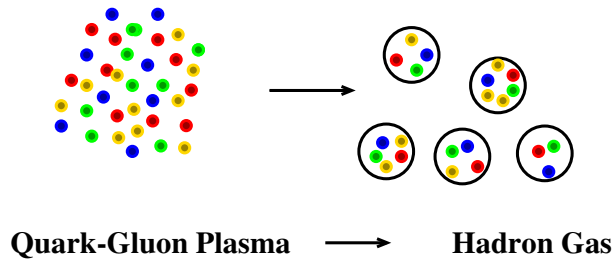


Fig. 1: As the energy density is decreased, the quark–gluon plasma condenses into a low-density gas of hadrons. Quarks are red, green, or blue and gluons are yellow.

make the matter have high enough energy density, the protons, nucleons, and other particles overlap and get squeezed so tightly that their constituents are free to roam the system without being confined inside hadrons [4]. At this density, there is deconfinement and the system is called a quark–gluon plasma. This is shown in Fig. 1.

As the energy density gets to be very large, the interactions between the quarks and gluons become weak. This is a consequence of the asymptotic freedom of strong interactions: at short distances the strong interactions become weak.

The QGP surely existed during the Big Bang. In Fig. 2, the various stages of evolution in the Big Bang are shown.

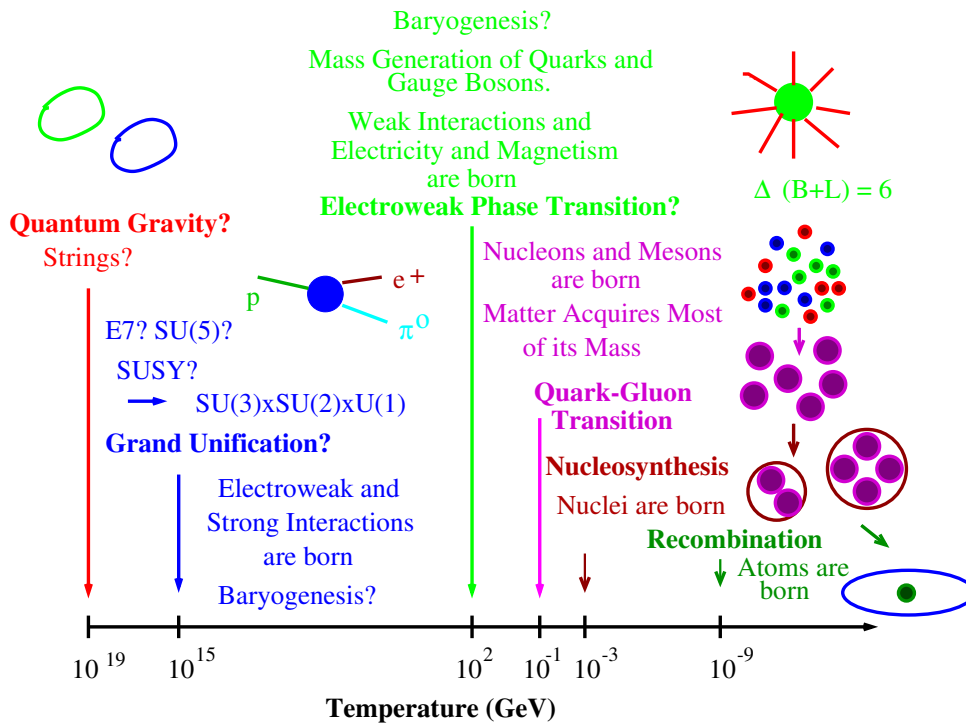


Fig. 2: The various forms of matter, and the types of physics which are probed during the Big Bang

At the earliest times in the Big Bang, temperatures are of order $T \sim 10^{19}$ GeV, quantum gravity is important, and despite the efforts of several generations of string theorists, we have little understanding. At somewhat lower temperatures, perhaps there is the grand unification of all the forces, except gravity. It might be possible that the baryon number of the universe is generated at this temperature scale. At much

lower temperatures, of order $T \sim 100$ GeV, electroweak symmetry breaking takes place. It is possible here that the baryon asymmetry of the universe might be produced. At temperatures of order $T \sim 1$ GeV, quarks and gluons become confined into hadrons. This is the temperature range appropriate for studies at RHIC and the LHC. At $T \sim 1$ MeV, the light elements are made. This temperature corresponds to an energy range which has been much studied, and is the realm of conventional nuclear physics. At temperatures of the order of an electronvolt, corresponding to the binding energies of electrons in atoms, the universe changes from an ionized gas to a lower-pressure gas of atoms, and structure begins to form.

The QGP is formed at energy densities of order $1 \text{ GeV}/\text{fm}^3$. Matter at such energy densities probably exists inside the cores of neutron stars as shown in Fig. 3. Neutron stars are objects of about

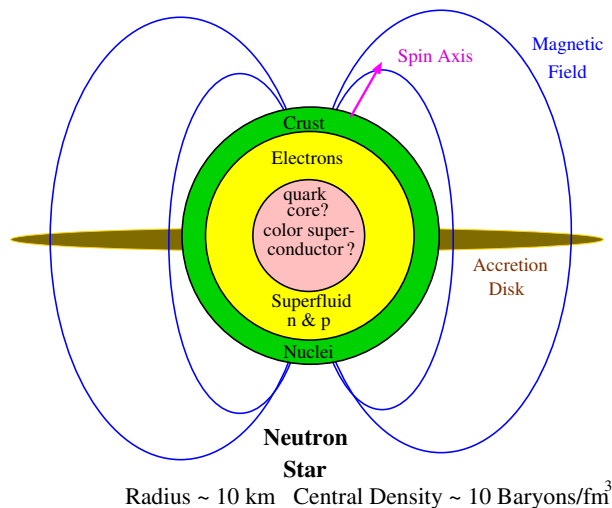


Fig. 3: A spinning neutron star

10 km in radius and are composed of extremely high energy density matter. The typical energy density in the core is of the order of $1 \text{ GeV}/\text{fm}^3$, and approaches zero at the surface. Unlike the matter in the Big Bang, this matter is cold and has temperature small compared to the Fermi energies of quarks. It is a cold, degenerate gas of quarks. At lower densities, this matter converts into a cold gas of nucleons.

Hot and dense matter with energy density of order $1 \text{ GeV}/\text{fm}^3$ may have occurred in the supernova explosion which led to the neutron star's formation. It may also occur in collisions of neutron stars and black holes, and may be the origin of the mysterious gamma-ray bursters. (Gamma-ray bursters are believed to be starlike objects which convert of the order of their entire mass into gamma rays.)

2.2.2 The quark–gluon plasma and ideal gases

At very high energy density, the coupling constant of QCD becomes weak. A gas of particles should to a good approximation become an ideal gas. Each species of particle contributes to the energy density of an ideal gas as

$$\epsilon = \int \frac{d^3p}{(2\pi)^3} \sum_i \frac{E_i}{e^{\beta E_i} \pm 1} \quad (2)$$

where the $-$ is for bosons and the $+$ for fermions. The energy of each particle is E_i . At high temperatures, masses can be ignored, and the factor of ± 1 in the denominator turns out to make a small difference. One finds therefore that

$$\epsilon \sim \frac{\pi^2}{30} NT^4 \quad (3)$$

where N is the number of particle degrees of freedom. At low temperatures when masses are important, only the lowest mass, strongly interacting particle degree of freedom contributes; the pion, and the energy density approaches zero as $\epsilon \sim e^{-m_\pi/T}$. For an ideal gas of pions, the number of pion degrees of freedom is three. For a QGP there are two helicities and eight colours for each gluon, and for each quark, three colours, two spins, and a quark–antiquark pair. The number of degrees of freedom is $N \sim 2 \times 8 + 4 \times 3 \times N_F$ where N_F is the number of important quark flavours, which is about three if the temperature is below the charm quark mass so that $N \sim 50$.

There is about an order of magnitude change in the number of degrees of freedom between a hadron gas and a QGP. This is because the degrees of freedom of the QGP include colour. In the large N_{colour} limit, the number of degrees of freedom of the plasma are proportional to N_{colour}^2 , and in the confined phase is of order 1. In this limit, the energy density has an infinite discontinuity at the phase transition. There would be a limiting temperature for the hadronic world in the limit for which $N_{\text{colour}} \rightarrow \infty$, since at some temperature the energy density would go to infinity. This is the Hagedorn limiting temperature. (In the real world N_{colour} is three, and there is a temperature at which the energy density changes by an order of magnitude in a narrow range.)

2.2.3 The quark–gluon plasma and fundamental physics issues

The nature of matter at high densities is an issue of fundamental interest. Such matter occurred during the Big Bang, and it is the ultimate and universal state of matter at very high energy densities.

A hypothetical phase diagram for QCD is shown in Fig. 4. The vertical axis is temperature, and the horizontal is a measure of the matter or baryon number density, the baryon number chemical potential [5]. The solid lines indicate a first-order phase transition, and the dashed line a rapid cross-over. It is not known for sure whether or not the region marked cross-over is or is not a true first-order phase transition. There are analytic arguments for the properties of matter at high density, but numerical computations are of insufficient resolution. At high temperature and fixed baryon number density, there are both analytic arguments and numerical computations of good quality. At high density and fixed temperature, one goes into a superconducting phase, perhaps multiple phases of superconducting quark matter. At high temperature and fixed baryon number density, the degrees of freedom are those of a quark–gluon plasma.

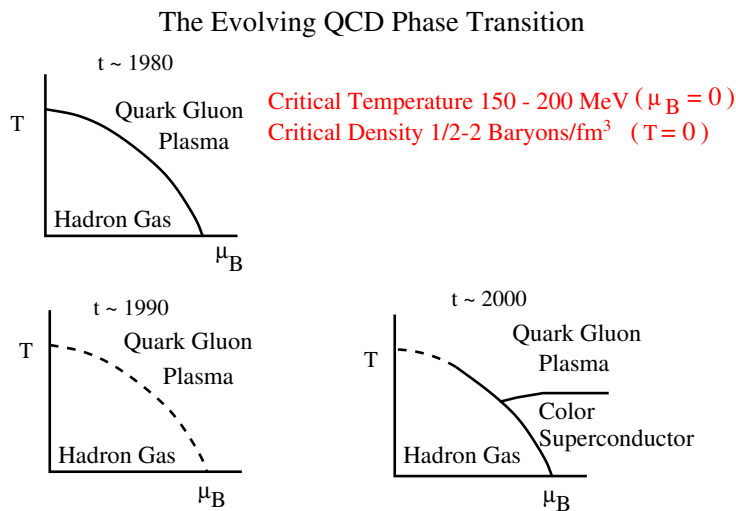


Fig. 4: A phase diagram for QCD collisions

I have shown this phase diagram as a function of time. What this means is that at various times people thought they knew what the phase diagram was. As time evolved, the picture changed. The latest

ideas are marked with the date 2000. The point of doing this is to illustrate that theoretical ideas in the absence of experiment change with time. Physics is essentially an experimental science, and it is very difficult to appreciate the richness which nature allows without knowing from experiment what is possible.

Much of the information we have about QCD at finite energy density comes from lattice gauge theory numerical simulation [5]. To see how lattice gauge theory works, recall that at finite temperature, the grand canonical ensemble is given by

$$Z = \text{Tr} e^{-\beta H} . \quad (4)$$

This is similar to computing

$$Z = \langle e^{-itH} \rangle \quad (5)$$

where $-it = \beta$. That is we compute the expectation value of the time evolution operator for imaginary time. This object has a path integral representation, which has been described to you in your elementary field theory text books. Under the change of variables, the action becomes $iS = i \int dt L \rightarrow S = - \int_0^\beta d\tau L$. Here L is the Lagrangian.

The grand canonical ensemble has the representation

$$Z = \int [dA] e^{-S[A]} \quad (6)$$

for a system of pure gluons. The gluon fields satisfy periodic boundary conditions due to the trace in the definition of the grand canonical ensemble. (Fermions may also be included, although the path integral is more complicated, and the fermion fields are required to satisfy antiperiodic boundary conditions.) Expectation values are computed as

$$\langle 0 \rangle = \frac{\text{Tr} O e^{-\beta H}}{\text{Tr} e^{-\beta H}} . \quad (7)$$

The way that lattice Monte Carlo simulates the grand canonical ensemble is by placing all of the fields on a finite grid, so the path integral becomes finite dimensional. Then field configurations are selectively sampled, as weighted by their action. This works because the factor of $e^{-\beta H}$ is positive and real. (The method has essential complications for finite density systems, since there the action becomes complex.)

Lattice gauge theory numerical studies, and analytic studies have taught us much about the properties of these various phases of matter [5]. There have been detailed computations of the energy density as a function of temperature. In Fig. 5 the energy density scaled by T^4 is plotted. This is essentially the number of degrees of freedom of the system as a function of T . At a temperature of $T_c \sim 160\text{--}190$ MeV the number of degrees of freedom changes very rapidly, possibly discontinuously. This is the location of the transition from the hadron gas to the quark–gluon plasma.

In Fig. 6, the sound velocity is plotted as a function of temperature. The sound velocity increases at high temperature asymptoting to its ideal gas value of $v_{\text{sound}}^2 \sim 1/3$. Near the phase transition, it becomes very small. This is because the energy density jumps at the transition temperature, but the pressure must be smooth and continuous. The sound velocity squared is $dP/d\epsilon$.

Lattice Monte Carlo simulation has also been used to study how the phase transition is related to the confining force. In a theory with only gluons, the potential for sources of fundamental representation colour charge grows linearly in the confined phase. (With dynamical fermions, the potential stops rising at some distance when it is energetically favourable to produce quark–antiquark pairs which short out the potential.)

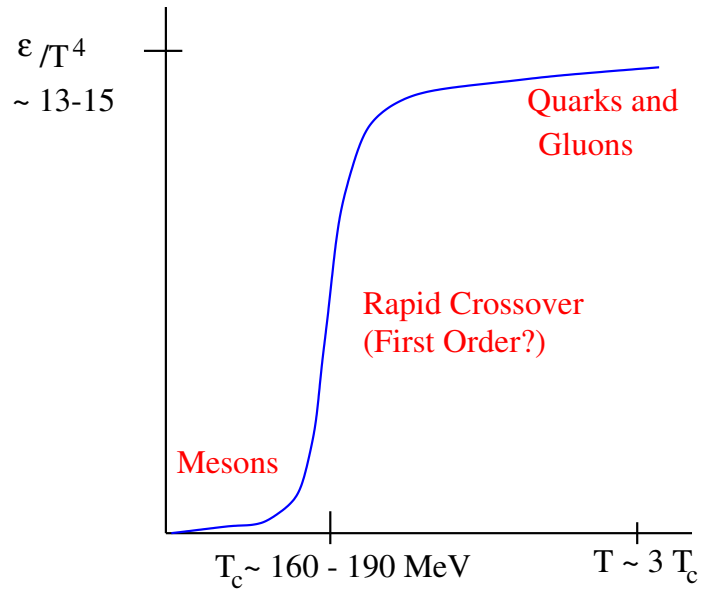


Fig. 5: The energy density scaled by T^4 as a function of temperature

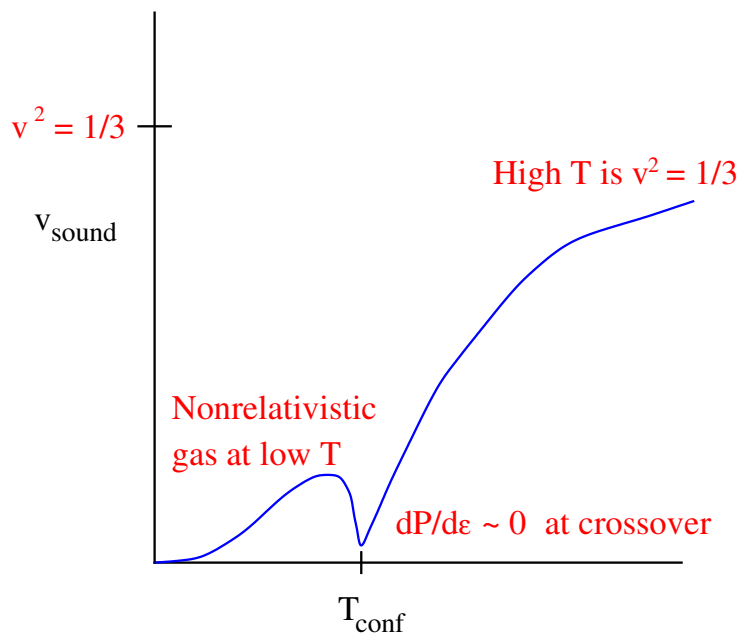


Fig. 6: The sound velocity as a function of temperature

We can understand how confinement might disappear at high temperature. At finite temperature, there is a symmetry of the pure gluon Yang–Mills system. Consider a Wilson line which propagates from $(0, \vec{x})$ to the point (β, \vec{x}) . A Wilson line is a path-ordered phase,

$$L(x) = P \exp i \int_0^\beta dt A^0(t, \vec{x}) . \quad (8)$$

One can show that the expectation value of this line gives the free energy of an isolated quark:

$$e^{-\beta F} = \frac{1}{N_c} \langle \text{Tr}(L(x)) \rangle . \quad (9)$$

Now consider gauge transformations which maintain the periodic boundary conditions on the gauge fields (required by the trace in the definition of the grand canonical ensemble). The most general gauge transformation which does this is not periodic but solves

$$U(\beta, \vec{x}) = ZU(0, \vec{x}). \quad (10)$$

One can show that $[z, \tau^a] = 0$, and that $\nabla^i Z = 0$. Z is an element of the gauge group so that $\det Z = 1$. These conditions require that

$$Z = e^{2\pi i j / N_c}. \quad (11)$$

This symmetry under non-periodic gauge transformations is global, that is it does not depend upon the position in space. It may be broken. If it is realized, the free energy of a quark must be infinite since $L \rightarrow ZL$ under this transformation, and $\langle L \rangle = 0$. If the symmetry is broken, quarks can be free.

Lattice gauge computations have measured the quark–antiquark potential as a function of T , and at the deconfinement temperature, the potential changes from linear at infinity to constant. This is shown in Fig. 7.

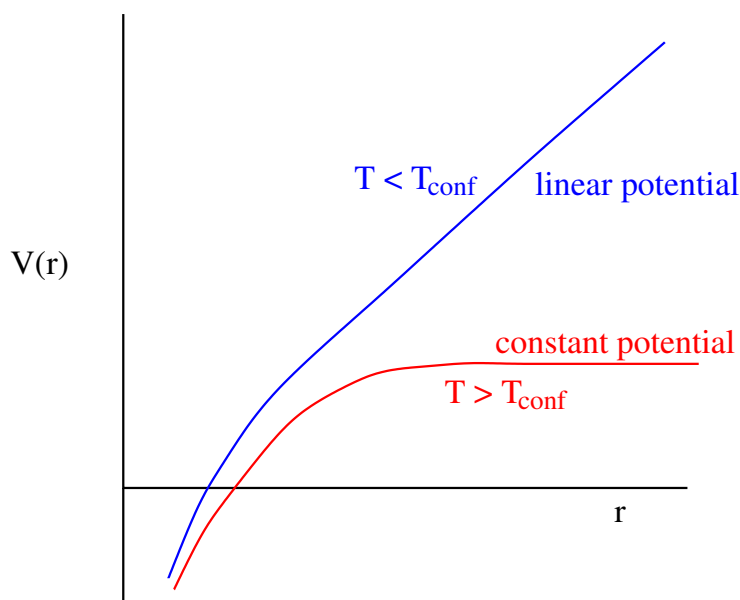


Fig. 7: The potential in pure gauge theory as a function of temperature

In addition to confinement–deconfinement, there is an additional symmetry which might occur at high temperatures. In nature, the up and down quark masses are almost zero. This leads to a chiral symmetry, which is the rotation of fermion fields by $e^{i\gamma_5 \theta}$. This symmetry would require that either baryons are massless or occur in parity doublets. Neither arises in nature. The nucleon has a mass of about 1 GeV and has no opposite parity partner of almost equal mass. It is believed that this symmetry becomes broken, and as a consequence, the nucleon acquires mass, and that the pion becomes an almost massless Goldstone boson. It turns out that at the confinement–deconfinement phase transition, chiral symmetry is restored. This is seen in Fig. 8 where a quantity proportional to the nucleon mass is plotted as a function of T .

The chiral symmetry restoration phase transition can have interesting dynamical consequences. In the confined phase, the mass of a nucleon is of order $N_c \Lambda_{\text{QCD}}$, but in the deconfined phase is of order T . Therefore in the confined phase, the Boltzman weight $e^{-M/T}$ is very small. Imagine what happens

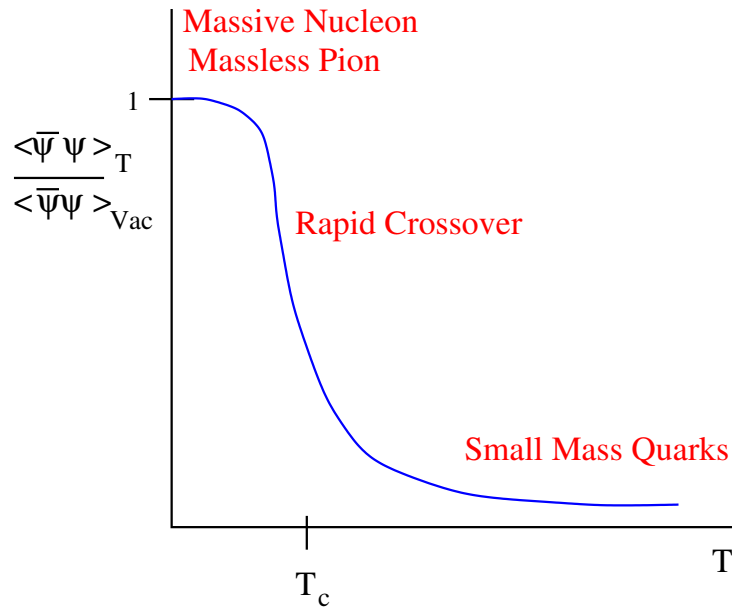


Fig. 8: The chiral order parameter $\langle \bar{\Psi} \Psi \rangle$ as a function of temperature

as we go through the phase transition starting at a temperature above T_c . At first the system is entirely in QGP. As the system expands, a mixed phase of droplets of QGP and droplets of hadron gas forms. The nucleons like to stay in the QGP because their Boltzmann weight is larger. As the system expands further, the droplets of QGP shrink, but most of the baryon number is concentrated in them. At the end of the mixed phase, one has made large-scale fluctuations in the baryon number. This scenario is shown in Fig. 9.

The confinement–deconfinement phase transition and the chiral symmetry restoration phase transition might be logically disconnected from one another. The confinement–deconfinement phase transition is related to a symmetry when the quark masses are infinite. The chiral transition is related to a symmetry when the quarks are massless. As a function of mass, one can follow the evolution of the phase transitions. At large and small masses there is a real phase transition marked by a discontinuity in physical quantities. At intermediate masses, there is probably a rapid transition, but not a real phase transition. It is believed that the real world has masses which make the transition closer to a cross-over than a phase transition, but the evidence from lattice Monte Carlo studies is very weak. In Fig. 10, the various possibilities are shown.

2.3 The colour glass condensate

This section describes the colour glass condensate, and why it is important for our understanding of basic properties of strong interactions [2], [6]. I argue that the colour glass condensate is a universal form of matter which controls the high-energy limit of all strong interaction processes and is the part of the hadron wavefunction important at such energies. Since the colour glass condensate is universal and controls the high-energy limit of all strong interactions, it is of fundamental importance.

2.3.1 What is the colour glass condensate?

The colour glass condensate is a new form of matter which controls the high-energy limit of strong interactions. It is universal and independent of the hadron which generated it. It should describe

- high-energy cross-sections

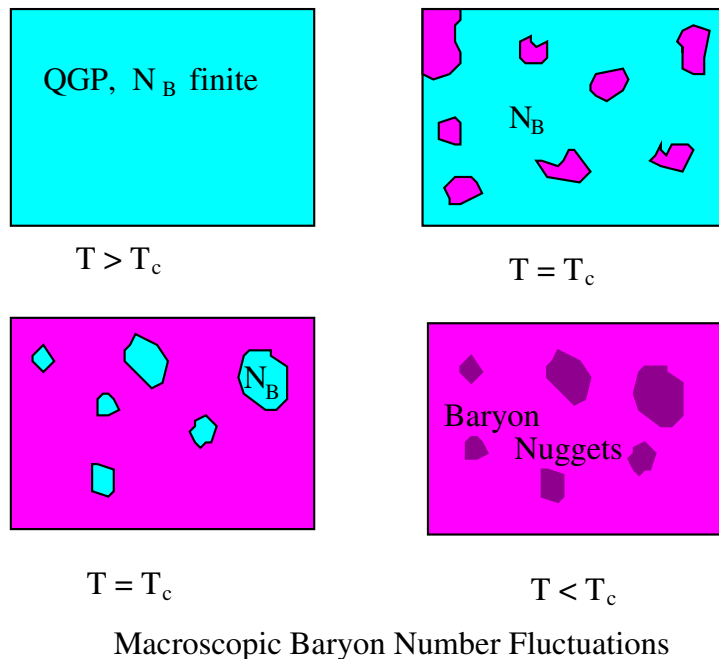


Fig. 9: Formation of large-scale baryon number fluctuations at the QCD phase transition

- distributions of produced particles
- the distribution of the small- x particles in a hadron
- initial conditions for heavy-ion collisions.

A very-high-energy hadron has contributions to its wavefunction from gluons, quarks, and anti-quarks with energies up to that of the hadron and all the way down to energies of the order of the scale of light-mass hadron masses, $E \sim 200$ MeV. A convenient variable in which to think about these quark degrees of freedom is the typical energy of a constituent scaled by that of the hadron,

$$x = E_{\text{constituent}}/E_{\text{hadron}} . \quad (12)$$

Clearly the higher the energy of the hadron we consider, the lower the minimum x of a constituent. Sometimes it is also useful to consider the rapidity of a constituent which is $y \sim \ln(1/x)$.

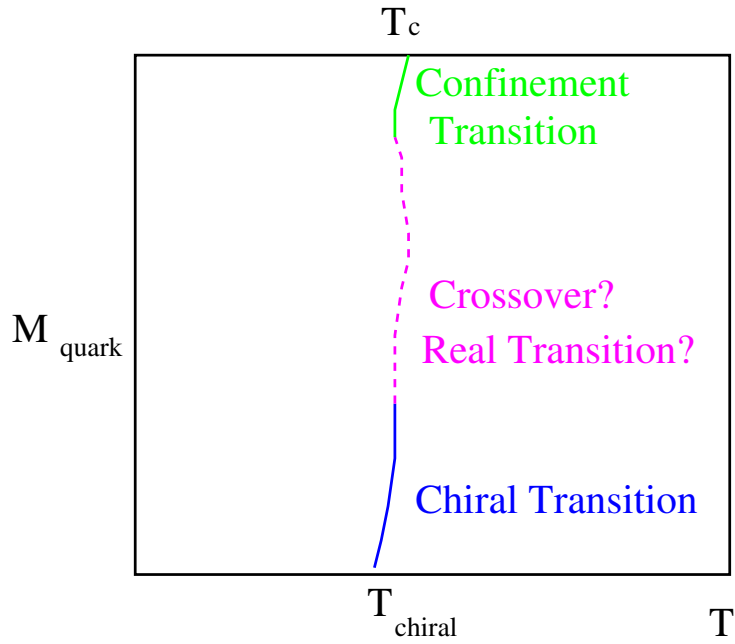
The density of small- x partons is

$$\frac{dN}{dy} = xG(x, Q^2) . \quad (13)$$

The scale Q^2 appears because the number of constituents one measures depends (weakly) upon the resolution scale of the probe with which one measures. (Resolution scales are measured in units of the inverse momentum of the probe, which is usually taken to be a virtual photon.) A plot of $xG(x, Q^2)$ for gluons at various x and Q^2 measured at the HERA accelerator in protons [7] is shown in Fig. 11.

Note that the gluon density rises rapidly at small x in Fig. 11. This is the so-called small- x problem. It means that if we view the proton head-on at increasing energies, the low-momentum gluon density grows. This is shown in Fig. 12.

As the density of gluons per unit area per unit rapidity increases, the typical transverse separation of the gluons decreases. This means that the matter which controls high-energy strong interactions is very dense, and it means that the QCD interaction strength which is usually parametrized by the dimensionless



The Pisarski Plot

Fig. 10: The phase diagram of QCD as a function of fermion mass

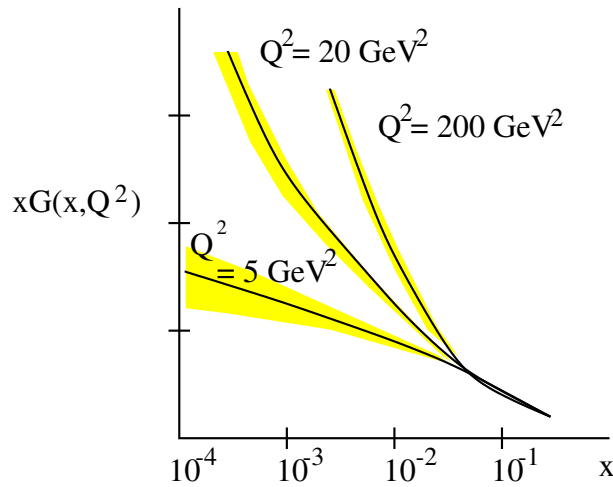


Fig. 11: The number of gluons in a proton per unit rapidity at various rapidities and Q^2 resolutions

scale α_s becomes small. The phase-space density of these gluons $\rho \sim 1/\pi R^2 dN/d^2p_T$ can become at most $1/\alpha_s$ since once this density is reached gluon interactions are important. This is characteristic of Bose condensation phenomena which are generated by an instability proportional to the density ρ and are compensated by interactions proportional to $\alpha_s \rho^2$, which become of the same order of magnitude when $\rho \sim 1/\alpha_s$. Thus the matter is a colour condensate.

The glassy nature of the condensate arises because the fields associated with the condensate are generated by constituents of the proton at higher momentum. These higher momentum constituents have their time scales Lorentz time dilated relative to those which would be measured in their rest frame. Therefore the fields associated with the low-momentum constituents also evolve on this long time scale.

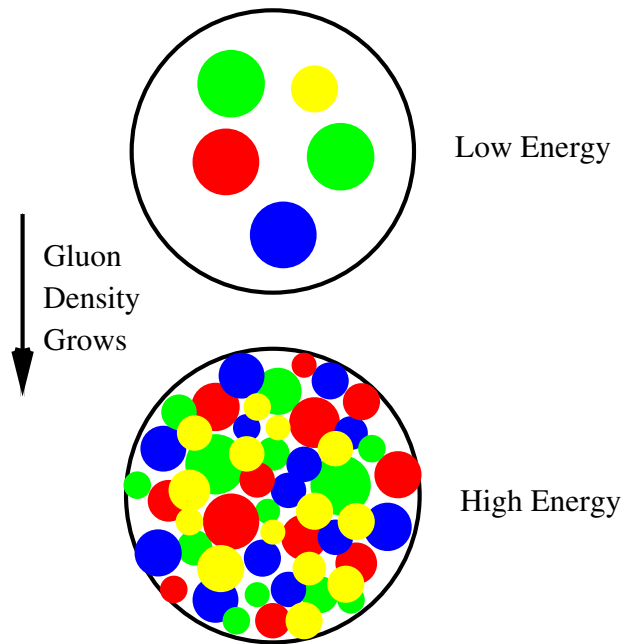


Fig. 12: The increasing density of wee partons as the energy increases

The low-momentum constituents are therefore glassy: their time evolution scale is unnaturally long compared to their natural time scale. Hence the name colour glass condensate.

There is also a typical scale associated with the colour glass condensate: the saturation momentum. This is the typical momentum scale where the phase-space density of gluons becomes $\rho \leq 1/\alpha_s$.

At very high momentum, the fields associated with the colour glass condensate can be treated as classical fields, like the fields of electricity and magnetism. Since they arise from fast moving partons, they are plane polarized, with mutually orthogonal colour electric and magnetic fields perpendicular to the direction of motion of the hadron. This is shown in Fig. 13.

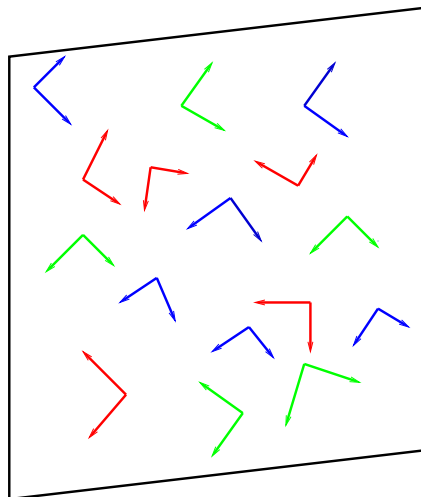


Fig. 13: The colour glass condensate as a high density of random gluon fields on a two-dimensional sheet travelling near the speed of light

2.3.2 Why is the colour glass condensate important?

Like nuclei and electrons compose atoms, and nucleons and protons compose nuclear matter, the colour glass condensate is the fundamental matter of which high-energy hadrons are composed. The colour glass condensate has the potential to allow for a first-principles description of the gross or typical properties of matter at high energies. For example, the total cross-section at high energies for proton–proton scattering, as shown in Fig. 14, has a simple form but for over 40 years has resisted simple explanation. (It has perhaps been understood recently in terms of the colour glass condensate or saturation ideas [8–11].)

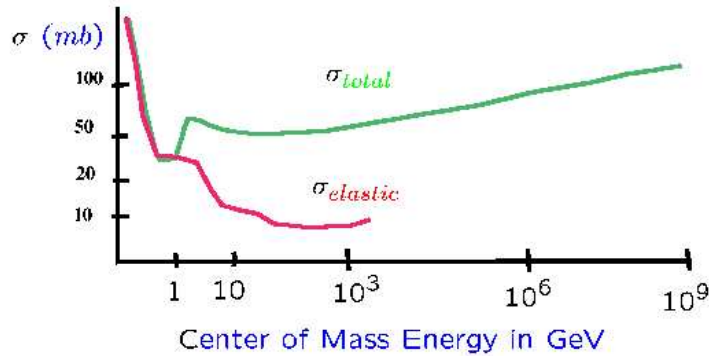


Fig. 14: The total cross-section for high-energy proton–proton interactions

The colour glass condensate forms the matter in the quantum mechanical state which describes a nucleus. In the earliest stages of nucleus–nucleus collisions, the matter must not be changed much from these quantum mechanical states. The colour glass condensate therefore provides the initial conditions for the quark–gluon plasma to form in these collisions. A space–time picture of nucleus–nucleus collisions is shown in Fig. 15. At very early times, the colour glass condensate evolves into a distribution of gluons. Later these gluons thermalize and may eventually form a quark–gluon plasma. At even later times, a mixed phase of plasma and hadronic gas may form.

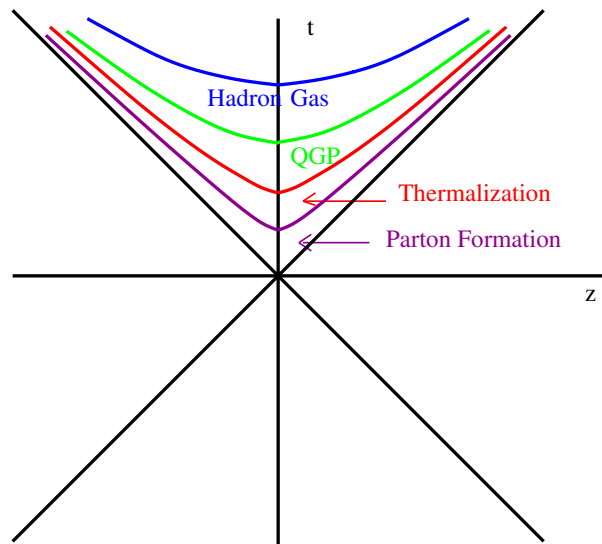


Fig. 15: A space–time diagram for the evolution of matter produced in heavy-ion collisions

2.4 The glasma

In collisions of nuclei, the matter inside a hadron is liberated. The matter immediately after the collision is called the glasma because it interpolates between the colour glass condensate in the initial nuclear wavefunction and the quark–gluon plasma. It has distinctive features which make it different from either the CGC or the QGP. In the colour glass condensate description, this may be thought of as the collision of two sheets of coloured glass, [12, 13], as shown in Fig. 16. When one writes down the equations which describe the evolution of the classical fields associated with the sheets of coloured glass, one finds that there is a discontinuity at $\tau = 0$. Immediately after the collision, the fields change their character, and instead of transverse colour electric and magnetic fields, with zero longitudinal fields, the fields transform into longitudinal colour electric and magnetic fields with zero transverse fields.

In low-energy, strong-interaction physics, one pictured collisions as generating a flux tube of colour electric field. In the high-energy limit, it seems one generates both longitudinal electric and magnetic fields. This is a consequence of the $E \leftrightarrow B$ duality symmetry of QCD.

One can see a consequence of a non-zero value of $E \cdot B$. Consider ordinary electricity and magnetism. An electric field accelerates an electron in one direction and B makes it spiral around with a specific handedness. For a positron, the acceleration is in the opposite direction, and so is the handedness. They therefore both generate the same chirality for an electron or a positron. In QCD, this works roughly the same way, and one can show that for strong values of $E \cdot B$, one can change the chirality of a system by spontaneous helicity flip induced by the field. $E \cdot B$ is proportional to a topological charge, which counts the number of such flips. Note that even though QCD in the limit of massless quarks has chiral symmetry, the topological charge can generate helicity flip processes. The topological charge is therefore related to anomalous processes, that is processes which are forbidden by the classical equations of motion.

In electroweak theory, a topological charge is generated in the Big Bang. This topological charge is associated with baryon number violation. It is possible that this topological charge generation is responsible for generating the baryon number of the universe.

When one writes down the Yang–Mills equations for these classical fields, the fields evolve in time. An example is the equation for the electric field,

$$D^0 \vec{E} = \vec{D} \times \vec{B} \quad (14)$$

where $D^0 = \delta^0 - igA^0$ is the covariant derivative operator. If there was only an electric field and no magnetic field, then the electric field could not decay classically, and would have to decay by pair creation. For the glasma, the fields can decay from classical dynamics.

Particles are produced when the fields become of low enough density so that they can be treated as linear wave equations. This is just like in electrodynamics where far away from sources, the equations are free equations and describe radiation.

These equations have been solved to describe the production of particles for high-energy nuclear collisions [12]. They are, however, unstable with respect to small fluctuations [14]. What this means is that if there are small fluctuations due to, for example, the quantum mechanical wavefunction of the initial state, these fluctuations form the seeds for chaotic evolution of the classical fields. Such chaotic configurations can thermalize the system, and some have speculated that this may be the origin of the rapid thermalization at RHIC.

3 Lecture II: Ultrarelativistic nuclear collisions

Heavy-ion collisions at ultrarelativistic energies are visualized in Fig. 16 as the collision of two sheets of coloured glass [12].

At ultrarelativistic energies, these sheets pass through one another. In their wake is left glasma, which eventually materializes as quarks and gluons. These quarks and gluons would naturally form in

their rest frame on some natural microphysics time scale. For the saturated colour glass, this time scale is of the order of the inverse saturation momentum (again, we convert momentum into time by appropriate uses of Planck’s constant and the speed of light), in the rest frame of the produced particle. When a particle has a large momentum along the beam axis, this time scale is Lorentz dilated. This means that the slow particles are produced first towards the centre of the collision regions and the fast particles are produced later further away from the collision region.

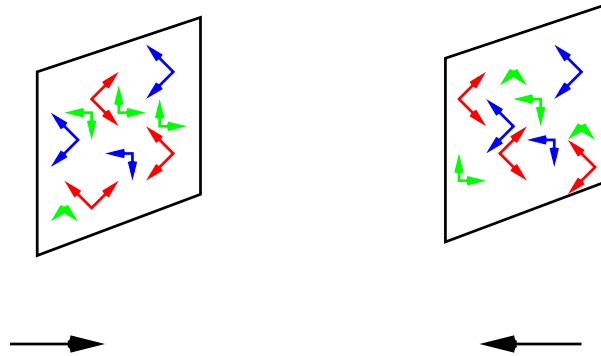


Fig. 16: The collision of two sheets of coloured glass

This correlation between space and momentum is similar to what happens to matter in Hubble expansion in cosmology. The stars which are further away have larger outward velocities. This means that this system, like the universe in cosmology is born expanding. This is shown in Fig. 17.

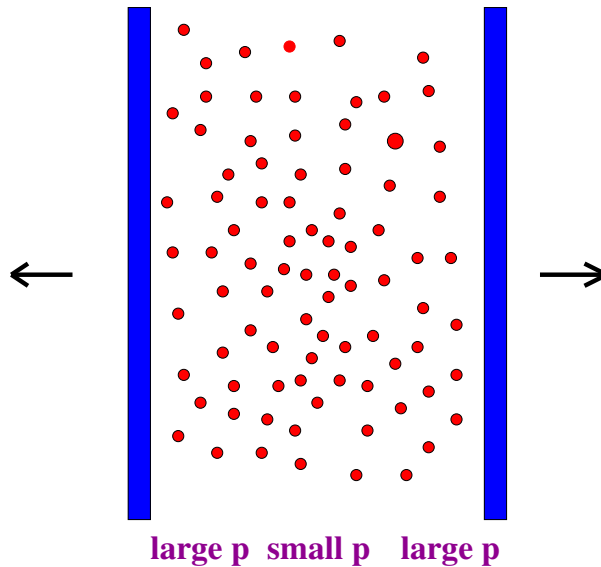


Fig. 17: Particles being produced after the collision of two nuclei

As this system expands, it cools. Presumably at some time the produced quarks and gluons thermalize. They then expand as a quark–gluon plasma and eventually as some mixture of hadrons and quarks and gluons. Finally, they may become a gas of only hadrons before they stop interacting and fly off to detectors.

In the last lecture, we shall describe the results from nucleus–nucleus collisions at RHIC in some detail. Before proceeding there, we need to learn a little bit more about the properties of high-energy hadrons. It is useful to introduce some kinematic variables which are useful in what will follow.

The light cone momenta are defined as

$$P^\pm = \frac{1}{\sqrt{2}}(E \pm p_z) \quad (15)$$

and light cone coordinates are

$$X^\pm = \frac{1}{\sqrt{2}}(t \pm z). \quad (16)$$

The metric in these variables is

$$p \cdot x = p^+ x^- + p^- x^+ - p_T \cdot x_T. \quad (17)$$

Conjugate variables are $x^\pm \langle - \rangle p^\mp$. The square of the four momentum is

$$p^2 = 2P^+ P^- - P_T^2 = M^2. \quad (18)$$

The uncertainty principle is

$$\Delta x^\pm \Delta p^\mp \geq 1. \quad (19)$$

Light cone variables are useful because in a high-energy collision, a left-moving particle has $p_z \sim E$, so that $p^+ \sim \sqrt{2}E$, but $p^- \sim m_T^2/p_z \sim 0$. For the right-moving particles, it is p^- which is big and p^+ which is very small.

Light cone variables scale by a constant under Lorentz transformations along the collision axis. Ratios of light cone momentum are therefore invariant under such Lorentz boosts. The light cone momentum fraction $x = p_i^+/P^+$, where P^+ is that of the particle we probe and p_i^+ is that of the constituent of the probed hadron, satisfies $0 \leq x \leq 1$. It is the same as Bjorken x , and for a fast-moving hadron, it is almost Feynman $x_{\text{Feynman}} = E_i/E$. This is the x variable one is using when one describes deep inelastic scattering. In this case the label i corresponds to a quark or gluon constituent of a hadron.

One can also define a rapidity variable:

$$y = \frac{1}{2} \ln \left\{ \frac{p_i^+}{p_i^-} \right\} \sim \ln(2E_i/M_T). \quad (20)$$

Up to mass effects, the rapidity is in the range $-y_{\text{proj}} \leq y \leq y_{\text{proj}}$. When particles, like pions, are produced in high-energy hadronic collisions, one often plots them in terms of the rapidity variable. Distributions tend to be slowly varying functions of rapidity.

3.1 Is there simple behaviour at high energy?

A hint of the underlying simplicity of high-energy hadronic interactions comes from studying the rapidity distributions of produced particles for various collision energies. In Fig. 18, a generic plot of the rapidity distribution of produced pions is shown for two different energies. The rapidity distribution at lower energies has been cut in half and the particles associated with each of the projectiles have been displaced in rapidity so that their starting points in rapidity are the same. It is remarkable that, except for the slowest particles in the centre-of-mass frame, those located near $y \sim 0$, the distributions are almost identical [15]. This is shown for the data from RHIC in Fig. 19.

We conclude from this that going to higher energy adds in new degrees of freedom, the small- x part of the hadron wavefunction. At lower energies, these degrees of freedom are not kinematically relevant as they can never be produced. On the other hand, going to higher energy leaves the fast degrees of freedom of the hadron unchanged.

This suggests that there should be a renormalization group description of the hadrons. As we go to higher energy, the high-momentum degrees of freedom remain fixed. Integrating out the previous small- x degrees of freedom should incorporate them into what are now the high-energy degrees of freedom at the higher energy. This process generates an effective action for the new low-momentum degrees of freedom. Such a process, when done iteratively, is a renormalization group.

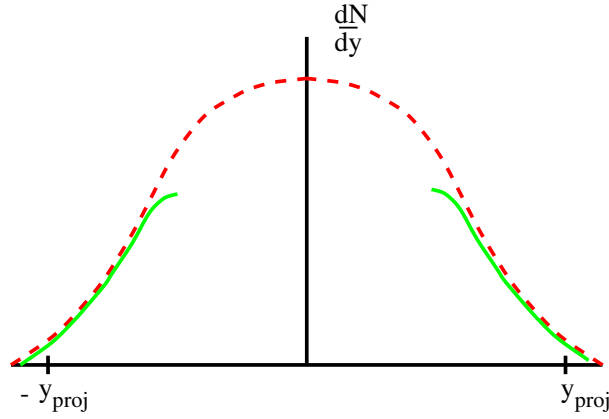


Fig. 18: The rapidity distributions of particles at two different energies

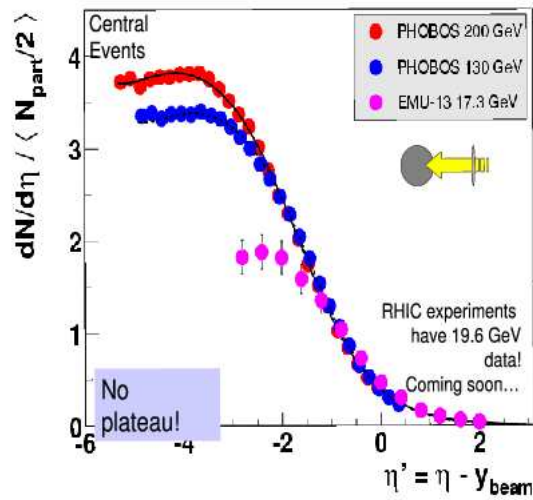


Fig. 19: Experimental evidence from the PHOBOS experiment at RHIC on limiting fragmentation

3.2 A single hadron

A plot of the rapidity distribution of the constituents of a hadron, the gluons, is shown generically in Fig. 20. I have used $y = y_{\text{hadron}} - \ln(1/x)$ as my definition of rapidity. This distribution is similar in shape to that of the half of the rapidity distribution shown for hadron–hadron interactions in the centre-of-mass frame which has positive rapidity. The essential difference is that this distribution is for constituents where the hadron–hadron collision is for produced particles, mainly pions.

In the high-energy limit, as discussed in the previous section, the density of gluons grows rapidly. This suggests we introduce a density scale for the partons

$$\Lambda^2 = \frac{1}{\pi R^2} \frac{dN}{dy}. \quad (21)$$

One usually defines a saturation momentum to be $Q_{\text{sat}}^2 \sim \alpha_s \Lambda^2$, since this will turn out to be the typical momentum of particles in this high-density system. In fact, α_s is slowly varying compared to the variation of Λ , so that for the purposes of the estimates we make here, whether or not there is a factor of α_s will not be so important. Note that α_s evaluated at the saturation scale will be $\alpha_s \ll 1$. The typical

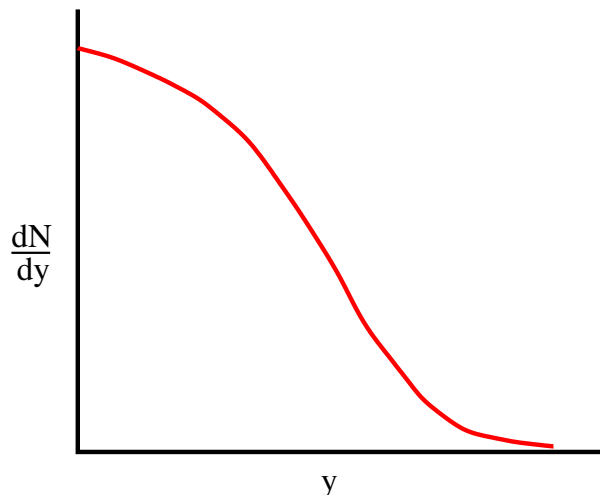


Fig. 20: The rapidity distribution of the constituents of a hadron

particle transverse momenta are of order $p_T^2 \sim Q_{\text{sat}}^2 \gg 1/R_{\text{had}}^2$. Therefore it is consistent to think of the parton distribution as a high-density, weakly coupled system which is localized in the transverse plane. The high-momentum partons, the degrees of freedom which should be frozen, can be thought of as sitting on an infinitesimally thin sheet. We shall study this system with a resolution size scale which is $\Delta x \ll 1/\Lambda_{\text{QCD}}$, so that we may use weak coupling methods. Such a thin sheet is shown in Fig. 21.

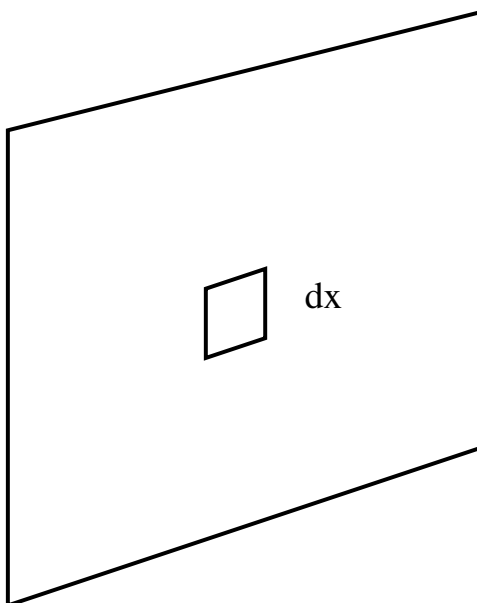


Fig. 21: A thin sheet travelling near light velocity. The transverse resolution scale is Δx .

It is useful to discuss different types of rapidity variables before proceeding. The typical momentum space rapidity is

$$y = \frac{1}{2} \ln \left(\frac{p^+}{p^-} \right)$$

$$\begin{aligned}
 &= \ln\left(\frac{2p^+}{M_T}\right) \\
 &= \ln\left(\frac{2p_{\text{hadron}}^+}{M_T}\right) + \ln\left(\frac{p^+}{p_{\text{hadron}}^+}\right) \\
 &= y_{\text{hadron}} - \ln(1/x) .
 \end{aligned} \tag{22}$$

Here M_T is a particle transverse mass, and we have made approximations which ignore overall shifts in rapidity by of order one unit. Within these approximations, the momentum space rapidity used to describe the production of particles is the same as that used to describe the constituents of hadrons.

Oftentimes a coordinate-space rapidity is introduced. With $\tau = \sqrt{t^2 - z^2}$,

$$y = \frac{1}{2} \ln\left(\frac{x^+}{x^-}\right) = \ln(2\tau/x^-) . \tag{23}$$

Taking τ to be a time scale of order $1/M_T$, and using the uncertainty principle $x^\pm \sim 1/p^\mp$, we find that up to shifts in rapidity of order one, all the rapidities are the same. This implies that coordinate space and momentum space are highly correlated, and that one can identify momentum-space and coordinate-space rapidity with some uncertainty of order one unit.

If we plot the distribution of particles in a hadron in terms of the rapidity variable, the longitudinal dimension of the sheet is spread out. This is shown in Fig. 22. The longitudinal position is correlated

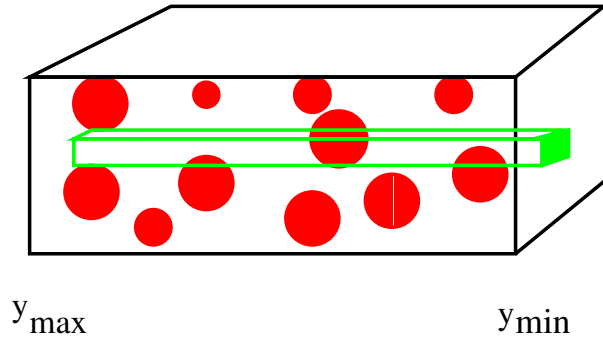


Fig. 22: The distribution of particles in a hadron in terms of rapidity variables

with the longitudinal momentum. The highest-rapidity particles are the fastest. In ordinary coordinate space, this means the fastest particles are those most Lorentz contracted. If we now look down a tube of transverse size $\Delta x \ll 1/\Lambda_{\text{QCD}}$, we intersect the various constituents of the hadron only occasionally. The colour charge probed by this tube should therefore be random, until the transverse size scale becomes large enough so that it can probe the correlations. If the beam energy is large enough, or x is small enough, there should be a large amount of colour charge in each tube of fixed size Δx . One can therefore treat the colour charge classically.

The physical picture we have generated is that there should be classical sources of to a good approximation random charges on a thin sheet. The current for this is

$$J_a^\mu = \delta^{\mu+} \delta(x^-) \rho_a(x_T) . \tag{24}$$

The delta function approximation should be good for many purposes, but it may also be useful in some circumstances to insert the longitudinal structure

$$J_a^\mu = \delta^{\mu+} \rho_a(y, x_T) \tag{25}$$

and to remember that the support of the source is for very large y .

3.3 The colour glass condensate

We now know how to write down a theory to describe the colour glass condensate. It is given by the path integral [6]

$$\int [dA][d\rho] \exp(iS[A, \rho] - W[\rho]). \quad (26)$$

Here $S[A, \rho]$ is the Yang–Mills action in the presence of a source current as described above. The function W weights the various configurations of colour charge. In the simplest version of the colour glass condensate, this can be taken to be a Gaussian

$$W = \frac{1}{2} \int dy d^2x_T \frac{\rho^2(y, x_T)}{\mu^2(y)}. \quad (27)$$

In this ansatz, $\mu^2(y)$ is the colour charge squared density per unit area per unit y scaled by $1/N_c^2 - 1$. The theory can be generalized to less trivial forms of the weight function, but this form works at small transverse resolution scales, $\Delta x \ll 1/Q_{\text{sat}}$. As one increases the transverse resolution scale one needs a better determination of W . It turns out that at resolution scales of order $1/Q_{\text{sat}} \ll \Delta x \ll 1/\Lambda_{\text{QCD}}$, a Gaussian form is still valid.

The averaging over an external field makes the theory of the colour glass condensate similar to that of spin glasses. The solutions of the classical field equations also have $F^2 \sim 1/\alpha$, so the gluon fields are strong and have high occupation number, hence the word condensate.

The theory described above has an implicit longitudinal momentum cutoff scale. Particles with momentum above this scale are treated as sources, and those below it as fields. One computes physical quantities by first computing the classical fields and then averaging over sources ρ . This is a good approximation so long as the longitudinal momentum in the field is not too far below the longitudinal momentum cutoff Λ^+ . If one computes quantum corrections, the expansion parameter is

$$\alpha_s \ln(\Lambda^+/p^+). \quad (28)$$

To generate a theory at smaller momenta $\bar{\Lambda}^+$ one first requires that $\alpha_s \ln(\Lambda^+/\bar{\Lambda}^+) \ll 1$. Then one computes the quantum corrections in the presence of the background field. This turns out to change only the weight function W . Therefore the theory maps into itself under a change of scale. This is a renormalization group, and it determines the weight function W [6], [16, 17].

3.4 Colour glass fields

The form of the classical fields is easily inferred. On either side of the sheet the fields are zero. They have no time dependence, and in light cone gauge $A^+ = 0$. It is plausible to look for a solution which is purely transverse. On either side of the sheet, we have fields which are gauge transformations of zero field. It can be a different gauge transformation of zero field on different sides of the sheet. Continuity requires that $F^{ij} = 0$. F^{i-} is zero because of light cone time x^+ independence, and the assumption that $A^- = 0$. F^{i+} is non-zero $\sim \delta(x^-)$ because of the variation in x^- as one crosses the sheet. This means that $F^{i0} \sim -F^{iz}$, or that $E \perp B \perp \vec{z}$. These are transversely polarized Weiszacker–Williams fields. They are random in the two-dimensional plane because the source is random. This is shown in Fig. 13. The intensity of these fields is of order $1/\alpha_s$, and they are not at all stringlike.

3.5 The gluon distribution and saturation

The gluon distribution function is given by computing the expectation value of the number operator $\langle a^\dagger(p)a(p) \rangle$ and can be found from computing the gluon field expectation value $\langle A(p)A(-p) \rangle$. This is

left as an exercise for the student. At large p_T , the distribution function scales as

$$\frac{dN}{dy d^2p_T} \sim \frac{1}{\alpha_s} \frac{Q_{\text{sat}}^2}{p_T^2} \quad (29)$$

which is typical of a bremsstrahlung spectrum. At small p_T , the solution is $\sim \ln(Q_{\text{sat}}^2/p_T^2)/\alpha_s$. The reason for this softer behaviour at smaller p_T is easy to understand. At small distances corresponding to large p_T , one sees point sources of charge, but at smaller p_T , the charges cancel one another and lead to a dipole field. The dipole field is less singular at large r , and when transformed into momentum space, one loses two powers of momentum in the distribution function. In terms of the colour field, the saturation phenomenon is almost trivial to understand. (It is very difficult to understand if the gluons are treated as incoherently interacting particles.)

Now Q_{sat}^2 can grow with energy. In fact it turns out that Q_{sat}^2 never stops growing. The intrinsic transverse momentum grows without bound. Physically what is happening is that the low-momentum degrees of freedom below the saturation momentum grow very slowly, like $\ln(Q_{\text{sat}}^2)$ because repulsive gluon interactions prevent more filling. On the other hand, one can always add more gluons at high momentum since the phase space is not filled there.

How is this consistent with unitarity? Unitarity is a statement about cross-sections at fixed Q^2 . If Q^2 is above the saturation momentum, then the gluon distribution function grows rapidly with energy, as Q_{sat}^2 . On the other hand, once the saturation momentum becomes larger than Q^2 , the number of gluons one can probe

$$xG(x, Q^2) \sim \pi R^2 \int_0^{Q^2} d^2p_T \frac{dN}{d^2p_T dy} \quad (30)$$

varies only logarithmically. The number of gluons scales as the surface area. (At high Q^2 , it is proportional to $R^2 Q_{\text{sat}}^2$, and one expects that $Q_{\text{sat}}^2 \sim A^{1/3}$ so that $xG(x, Q^2) \sim A$.)

3.6 Hadron collisions

In Fig. 16, the collision of two hadrons is represented as that of two sheets of coloured glass. Before the collisions, the left-moving hadron has fields

$$\begin{aligned} F^{i+} &\sim \delta(x^-) \\ F^{ij} &\sim 0 \\ F^{i-} &\sim 0 \end{aligned} \quad (31)$$

and that of the right-moving fields is analogous to that of the above save that $\pm \rightarrow \mp$ in the indices and coordinates of all fields. The fields are of course different in each nucleus. We shall consider impact-parameter-zero head-on collisions in what follows.

These fields are plane polarized and have random colours. A solution of the classical Yang–Mills equation can be constructed by requiring that the fields be two-dimensional gauge transforms of vacuum everywhere but in the forward light cone. At the edges of the light cone, and at its tip $t = z = 0$, the equations are singular, and a global solution requires that the fields carry non-trivial energy and momentum in the forward light cone. At short times, these fields are highly non-linear. In a time of order $\tau \sim 1/Q_{\text{sat}}$, the fields linearize. When they linearize, we can identify the particle content of the classical radiation field.

The solution to this classical field theory problem is the glasma. The fields have a discontinuity at $t = 0$ where the transverse fields are converted into longitudinal fields. These fields have non-zero $\vec{E} \cdot \vec{B}$ and, as described at the end of the last section, carry a non-zero topological charge. During the

time evolution of the glasma, there are both gluonic and quark degrees of freedom, and large coherent colour electric and magnetic fields.

This situation is much different than the case for quantum electrodynamics. Because of the gluon self-interaction, it is possible to classically convert the energy in the incident nuclei into radiation. In quantum electrodynamics, the charged particles are fermions, and they cannot be treated classically. Radiation is produced by annihilation or bremsstrahlung as quantum corrections to the initial value problem.

The solution to the field equation in the forward light cone is approximately boost invariant over an interval of rapidity of order $\Delta y \ll 1/\alpha_s$. At large momentum, the field equations can be solved in perturbation theory and the distribution is like that of a bremsstrahlung spectrum

$$\frac{dN}{dy d^2p_T} \sim \frac{1}{\alpha_s} \pi R^2 \frac{Q_{\text{sat}}^4}{p_T^4}. \quad (32)$$

It can be shown that such a spectrum matches smoothly onto the result for high-momentum-transfer jet production.

One of the outstanding problems of particle production is computing the total multiplicity of produced gluons. In the CGC description, this problem is solved. When $p_T \leq Q_{\text{sat}}$, non-linearities of the field equations become important, and the field stops going as $1/p_T^4$. Instead it becomes of order

$$\frac{dN}{dy d^2p_T} \sim \frac{1}{\alpha_s} \pi R^2. \quad (33)$$

The total multiplicity is therefore of order

$$N \sim \frac{1}{\alpha_s} \pi R^2 Q_{\text{sat}}^2. \quad (34)$$

If $Q_{\text{sat}}^2 \sim A^{1/3}$, then the total multiplicity goes as A , the high- p_T differential multiplicity goes as $A^{4/3}$, as we naively expect for hard processes since they should be incoherent, and the low-momentum differential multiplicity goes as $A^{2/3}$, since these particles arise from the region where the hadrons are black disks and the emission should take place from the surface.

In Fig. 23, the various kinematic regions for production of gluons are shown. In Fig. 24, the results

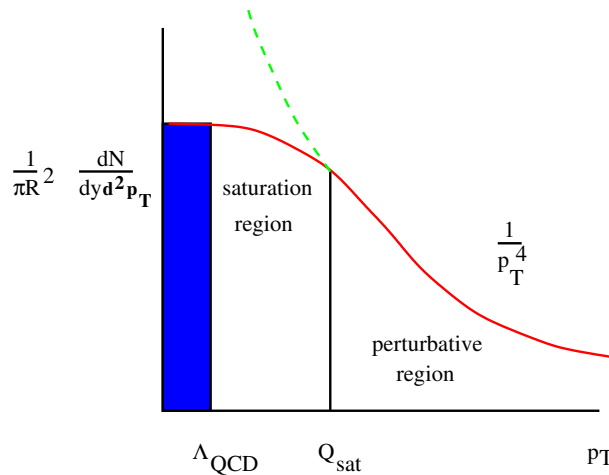


Fig. 23: A cartoon representation of the various kinematic regions of gluon production

of numerical simulation of gluon production are shown. At small p_T , it is amusing that the distribution is well described by a two-dimensional Bose–Einstein distribution. This is presumably a numerical accident, and in this computation has absolutely nothing to do with thermalized distributions.

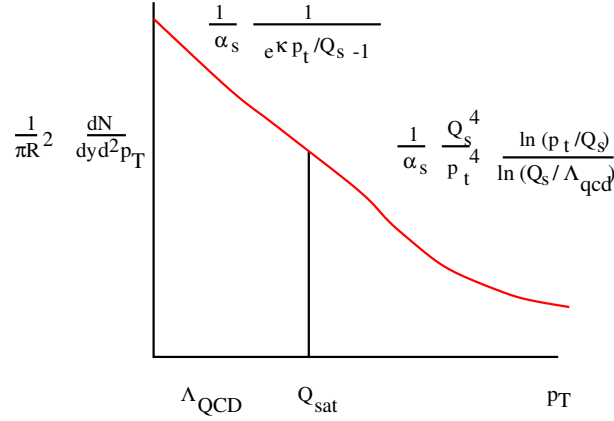


Fig. 24: The numerically computed distribution of produced gluons

3.7 Thermalization

As shown in Fig. 17, in a heavy-ion collision, the slow particles are produced first near the collision point and the slow particles are produced later far from the collision point. This introduces a gradient into the initial matter distribution, and the typical comoving volume element expands like $1/\tau$. To understand the factor of $1/\tau$ in the above equation, note that if we convert $dN/dz = dN/dy$, $dy/dz = dN/dy 1/t$, where we used our previous definition of space-time rapidity, and where we evaluated at $z = 0$. This is the physical rest frame density at $z = 0$.

If entropy is conserved, as is the case for a thermalized system with expansion time small compared to collision time,

$$S \sim T^3 \tau R^2 \quad (35)$$

is fixed so that $T \sim 1/\tau^{1/3}$. Therefore for a thermalized system, the energy density decreases as $\epsilon \sim 1/\tau^{4/3}$ for a system with no scattering so that the typical transverse momentum does not change, $\epsilon \sim 1/\tau$.

For the initial conditions typical of a colour glass condensate, thermalization is not so easy to do [18]. At the earliest times, the typical transverse momentum is large, of order of the saturation momentum. At this scale, the coupling is weak $\alpha_s(Q_{\text{sat}}) \ll 1$, at least for asymptotically large energy. It is believed by some that thermalization might be achieved in the glasma due to instabilities of the classical equations of motion [14]. The simple boost invariant solution to the classical equations described above is unstable if one allows small rapidity dependent fluctuations. These fluctuations grow with time, generating large fields. These fields strongly influence the motion of the gluon and quark degrees of freedom. A chaotic or turbulent fluid is generated, and this fluid might thermalize itself through the interactions of the unstable modes with the gluon and quark degrees of freedom.

The details of how this thermalization occurs have not been fully worked out in detail. Current estimates of the time of thermalization matter produced in heavy-ion collisions at RHIC energies range from $0.3 \leq \tau \leq 3 \text{ fm}/c$.

4 Lecture III: What we have learned from RHIC

In this lecture, I review results from RHIC and describe what we have learned so far about the production of new forms of matter in heavy-ion collisions. I shall make the case that we have produced matter of extremely high energy density, so high that it is silly not to think of it as composed of quarks and gluons. I shall also argue that this matter is strongly interacting with itself. The issue of the properties of this matter is still largely unresolved. For example, whether the various quantities measured are more

properly described as arising from a colour glass condensate or from a quark–gluon plasma, although we can easily understand in most cases which form of matter should be most important.

The data presented here are taken from the RHIC whitepapers [15]. For references to the original publications, please look there.

4.1 The energy density is big

The particle multiplicity as a function of energy has been measured at RHIC, as shown in Fig. 25. Combining the multiplicity data together with the measurements of transverse energy or of typical parti-

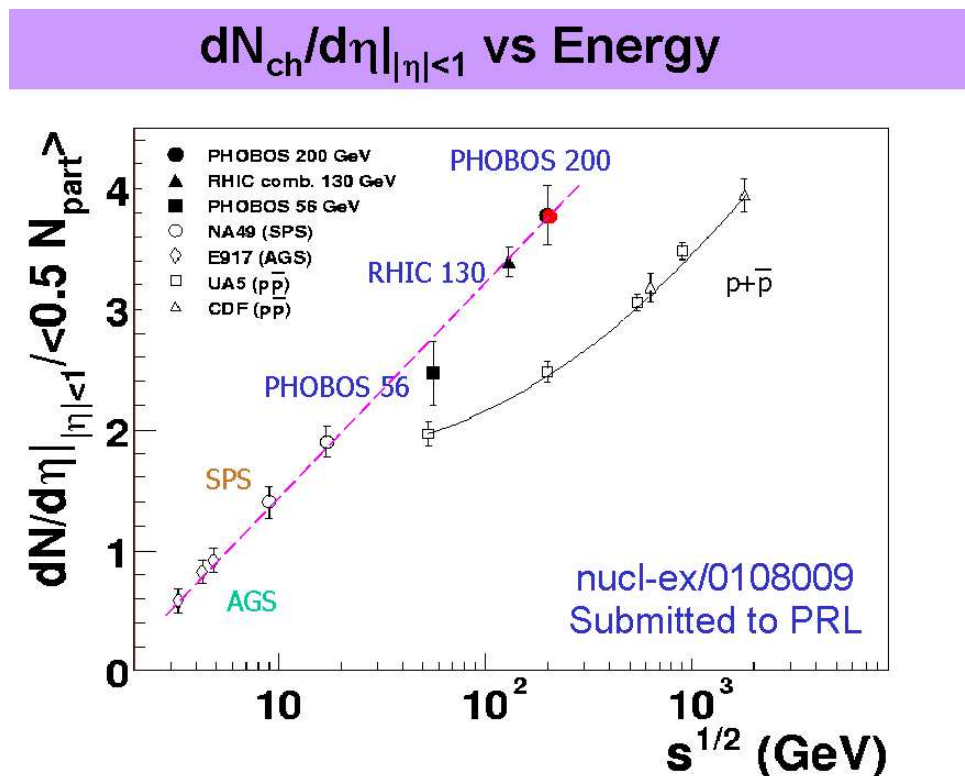


Fig. 25: Particle multiplicity as a function of energy as measured at RHIC

cle transverse momenta, one can determine the energy density of the matter when it decouples [15]. One can then extrapolate backwards in time. We extrapolate backwards using one-dimensional expansion, since decoupling occurs when the matter first begins to expand three dimensionally. We can extrapolate backwards until the matter has melted from a colour glass.

To do this extrapolation we use that the density of particles falls as $N/V \sim 1/t$ during one-dimensional expansion. If the particles expand without interaction, then the energy per particle is constant. If the particles thermalize, then $E/N \sim T$, and since $N/V \sim T^3$ for a massless gas, the temperature falls as $T \sim t^{-1/3}$. For a gas which is not quite massless, the temperature falls somewhere in the range $T_o > T > T_o(t_o/t)^{1/3}$, that is the temperature is bracketed by the value corresponding to no interaction and to that of a massless relativistic gas. This one-dimensional expansion continues until the system begins to feel the effects of finite size in the transverse direction, and then rapidly cools through three-dimensional expansion. Very close to when three-dimensional expansion begins, the system decouples and particles free-stream to detectors without further interaction. We shall take a conservative overestimate of this time to be of order $t_{melt} \sim 0.3$ fm/c. The extrapolation backwards is bounded by $\epsilon_f(t_f/t) < \epsilon(t) < \epsilon_f(t_f/t)^{4/3}$. The lower bound is that assuming that the particles do not thermalize

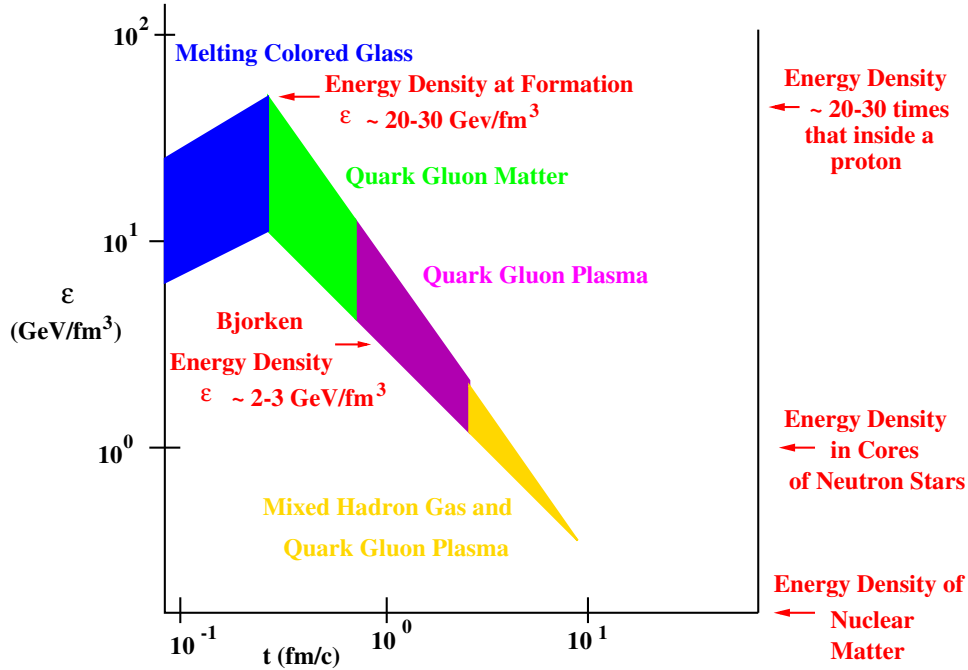


Fig. 26: Bounds on the energy density as a function of time in heavy-ion collisions

and their typical energy is frozen. The upper bound assumes that the system thermalizes as an ideal massless gas. We argued above that the true result is somewhere in between. When the time is as small as the melting time, then the energy density begins to decrease as time is further decreased.

This bound on the energy density is shown in Fig. 26. On the left axis is the energy density and on the bottom axis is time. The system begins as a colour glass condensate, then melts to quark–gluon matter which eventually thermalizes to a quark–gluon plasma. At a time of a few fm/c, the plasma becomes a mixture of quarks, gluons, and hadrons which expand together.

At a time of about 10 fm/c, the system falls apart and decouples. At a time of $t \sim 1$ fm/c, the estimate we make is identical to the Bjorken energy density estimate, and this provides a lower bound on the energy density achieved in the collision. (All estimates agree that by a time of order 1 fm/c, matter has been formed.) The upper bound corresponds to assuming that the system expands as a massless thermal gas from a melting time of 0.3 fm/c. (If the time was reduced, the upper bound would be increased yet further.) The bounds on the energy density are therefore

$$2\text{--}3 \text{ GeV/fm}^3 < \epsilon < 20\text{--}30 \text{ GeV/fm}^3 \quad (36)$$

where we included a greater range of uncertainty in the upper limit because of the uncertainty associated with the formation time. The energy density of nuclear matter is about 0.15 GeV/fm^3 , and even the lowest energy densities in these collisions is in excess of this. At late times, the energy density is about that of the cores of neutron stars, $\epsilon \sim 1 \text{ GeV/fm}^3$.

At such extremely high energy densities, the matter is most simply described in terms of its quark and gluon degrees of freedom.

4.2 The gross features of multiplicity distributions are consistent with coloured glass

As argued by Kharzeev and Nardi [19], the density of produced particles per nucleon which participates in the collision N_{part} should be proportional to $1/\alpha_s(Q_{\text{sat}})$, and $Q_{\text{sat}}^2 \sim N_{\text{part}}$. This dependence follows from the $1/\alpha_s$ which characterizes the density of the colour glass condensate. In Fig. 27, we show the

$dN/d\eta$ vs Centrality at $\eta=0$

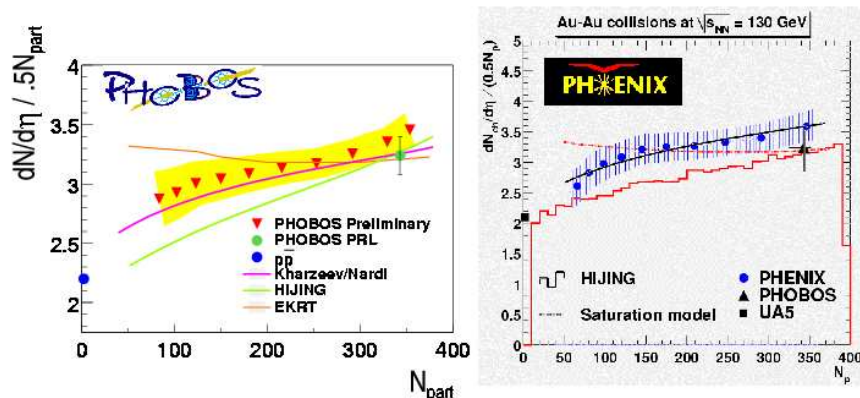


Fig. 27: The CGC description of the participant dependence of the multiplicity of produced particles

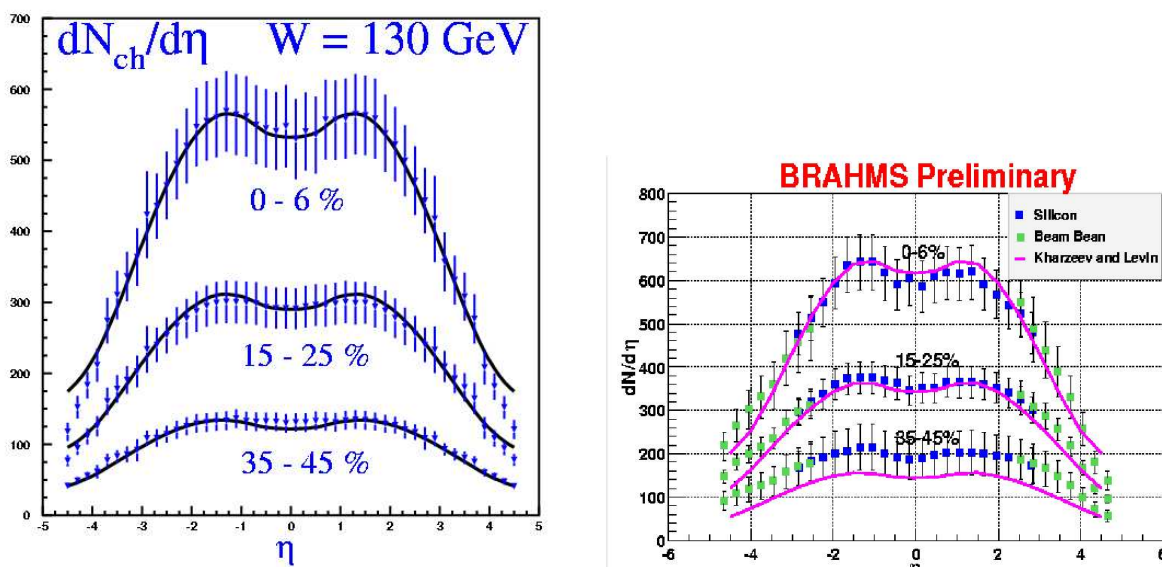


Fig. 28: Colour glass condensate fits to the rapidity density measured in the PHOBOS and BRAHMS experiments

data from PHENIX and PHOBOS [15]. The Kharzeev–Nardi form fits the data well. Other attempts such as HIJING [20], or the so-called saturation model of Eskola–Kajantie–Ruuskanen–Tuominen [21] are also shown in the figure. Kharzeev and Levin have recently argued that the rapidity distributions as a function of centrality can be computed from the colour glass description [22]. This is shown in Fig. 28.

4.3 The CGC describes features of deep inelastic scattering

The colour glass condensate provides a theory of the hadron wavefunction at very small values of x . As such, it should describe features not only of high-energy nucleus–nucleus scattering, but also electron–hadron scattering. This includes inclusive scattering and diffraction. It indeed appears that there is such a successful phenomenology [23].

In these notes, I shall describe only one aspect of this phenomenology, geometric scaling [24]–[27]. The basic idea is that the cross-section for virtual photon scattering from a hadron should be, up to some trivial overall scale factor, a dimensionless function. If the saturation momentum is the only scale in the problem and the properties of the matter probed depend only upon the density of the matter, then

$$\sigma_{\gamma^*p} \sim F(Q^2/Q_{\text{sat}}^2(x)) \quad (37)$$

and is not an independent function of x and Q^2 . The dependence of the saturation momentum on x can be computed [28], or can be determined from data. In Fig. 29, this cross-section is plotted as a function

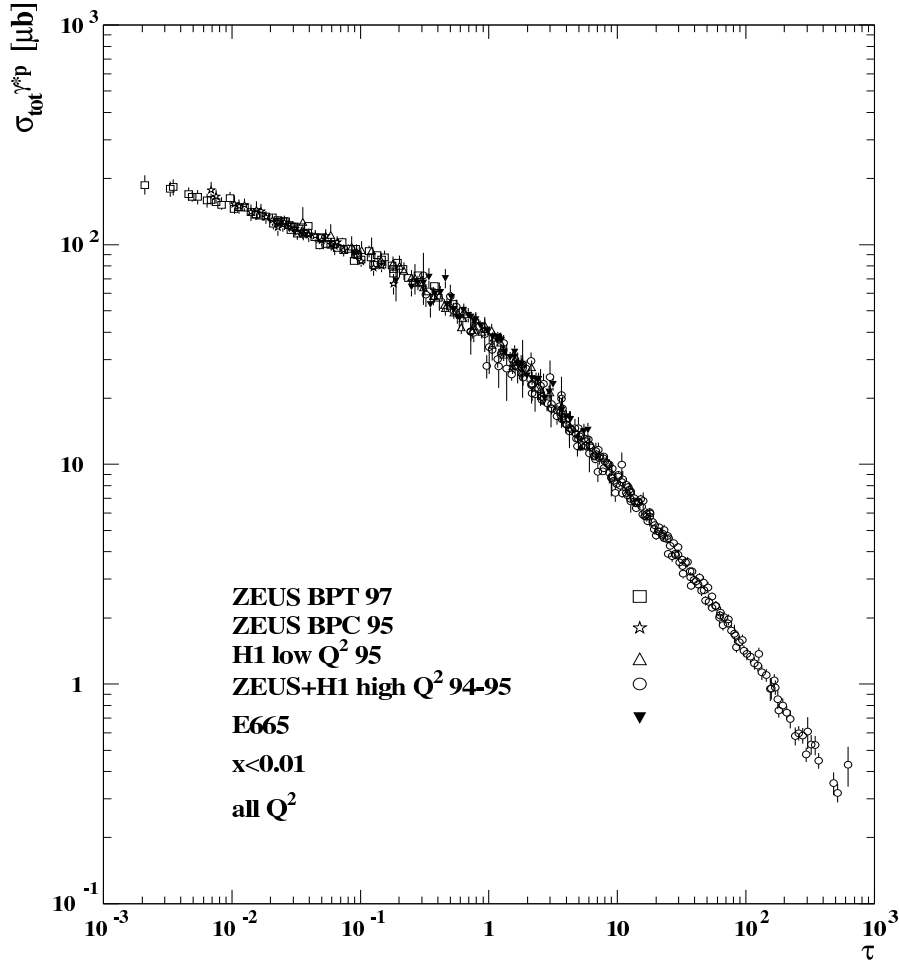


Fig. 29: The cross-section σ_{γ^*p} as a function of τ for $x \leq 10^{-2}$

of $\tau = Q^2/Q_{\text{sat}}^2$ for values of $x \leq 10^{-2}$. Indeed, there appears to be such scaling.

While it is easy to understand this scaling for $Q^2 \leq Q_{\text{sat}}^2$, it is perhaps a little surprising that it works to much larger values of Q^2 . One can show that one expects approximate scaling up to $Q^2 \sim Q_{\text{sat}}^4/\Lambda_{\text{QCD}}^2$. However, one should and can compute scaling violations [27].

4.4 The CGC provides a theory of shadowing

The naive expectation for the production of hard particles from a nucleus is that they should be generated by incoherent scattering. This is, however, modified because of multiparticle scattering, and because the gluon distribution function itself acquires a non-trivial dependence upon the nuclear baryon number. The colour glass condensate provides a theory of this modification [29–34].

One can understand how this works by first considering the effects of multiple elastic scattering. Such scattering does not change the number of particles. At very high p_T , the effects of multiple scattering should be small, since cross-sections are small. At intermediate p_T , the p_T distribution in a nucleus should broaden relative to that of incoherent scattering from nucleons. By conservation of probability, this requires a suppression at low p_T . By similar reasoning, one expects that these effects will be accentuated as one goes from peripheral to more central collisions. The results of one such computation of multiple scattering are shown in Fig. 30 [35].

One also expects that the effects of multiple scattering will be larger at small values of x because there are more degrees of freedom to scatter from.

Such multiple-scattering effects are included in the CGC description of the hadron collisions, but there is another effect which is larger at very small x . This is the quantum evolution of the hadron wavefunction. Because the saturation momentum is larger in nuclei than it is in protons, it is more difficult to produce glue at small x . Therefore as one goes to smaller values of x , there should be fewer particles at small x relative to the expectation from incoherent scattering. In Fig. 31, p_T distributions as a function of x are shown for the ratio of hadron–nucleus collisions to incoherent scattering. At large values of x there is a clear Cronin enhancement. At small values of x , there is a suppression as predicted by quantum evolution in the CGC. There is a similar suppression as the centrality of the collisions increases in distinction from the effects of multiple elastic scattering.

In the BRAHMS experiment, dAu collisions were used to study this effect. The results are shown in Fig. 32 [15]. Similar results have been found by STAR and PHENIX [15]. The results are qualitatively in accord with the CGC expectations, and also exhibit semi-quantitative agreement [36].

4.5 Matter has been produced which interacts strongly with itself

In off-zero-impact-parameter heavy-ion collisions, the matter which overlaps has an asymmetry in density relative to the reaction plane. This is shown in the left-hand side of Fig. 33. Here the reaction plane is along the x axis. In the region of overlap there is an x – y asymmetry in the density of matter which overlaps. This means that there will be an asymmetry in the spatial gradients which will eventually transmute itself into an asymmetry in the momentum space distribution of particles, as shown in the right-hand side of Fig. 33.

This asymmetry is called elliptic flow and is quantified by the variable v_2 . In all attempts to theoretically describe this effect, one needs very strong interactions among the quarks and gluons at very early times in the collision [37]. In Fig. 34, two different theoretical descriptions are fit to the data by STAR and PHOBOS [15]. On the left-hand side, a hydrodynamical model is used [38]. It is roughly of the correct order of magnitude and has roughly the correct shape to fit the data. This was not the case at lower energy. On the right-hand side are preliminary fits assuming colour glass [39]. Again it has roughly the correct shape and magnitude to describe the data. In the colour glass, the interactions are very strong essentially from $t = 0$, but unlike the hydrodynamic models it is field pressure rather than particle pressure which converts the spatial anisotropy into a momentum space-anisotropy.

Probably the correct story for describing flow is complicated and will involve both the quark–gluon plasma and the colour glass condensate. Either description requires that matter be produced in the collisions and that it interact strongly with itself. In the limit of single scatterings for the partons in the two nuclei, no flow is generated.

Recent data on charm particles show that they too flow with the produced matter [40, 41]. Charm is a very heavy particle, and as such it requires many collisions with other particles before it can flow with the surrounding matter. The amount of flow seen experimentally exceeds the wildest expectations of theorists.

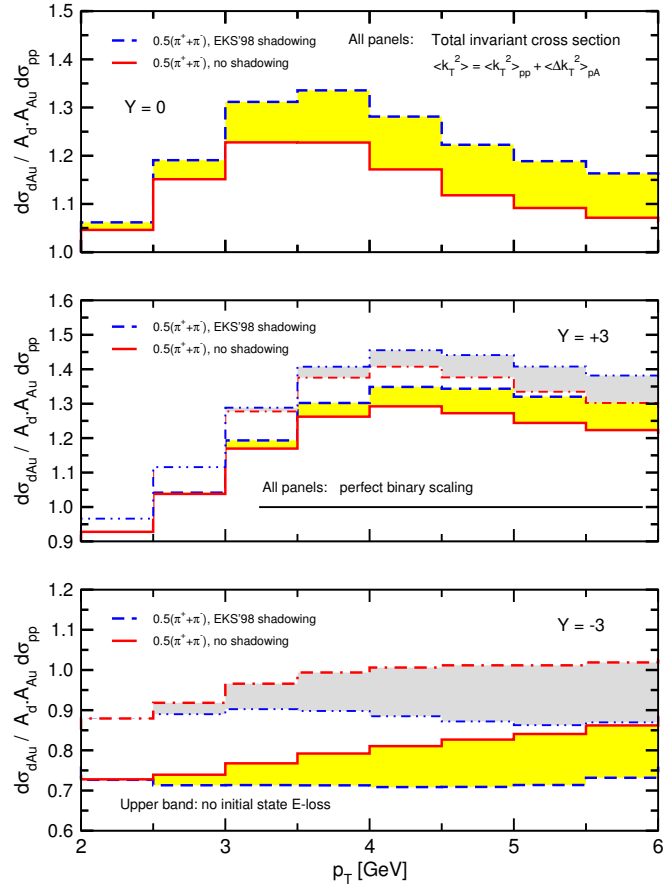


Fig. 30: The expectations of multiple scattering in dAu collisions in a multiple-scattering computation

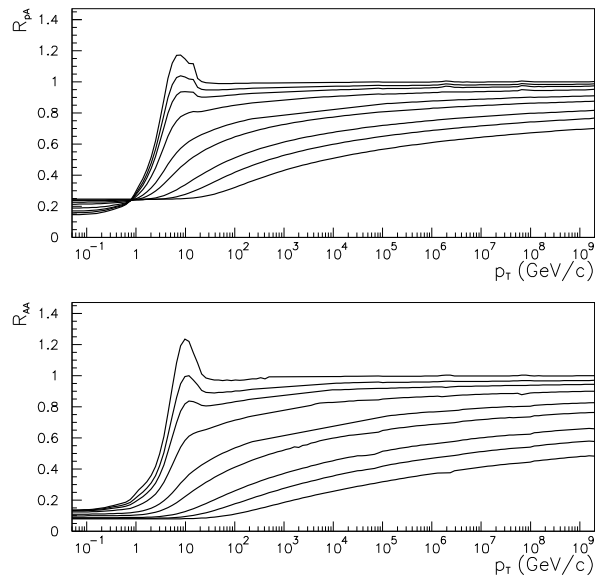


Fig. 31: The p_T distributions in hadron–nucleus collisions relative to incoherent scattering. Different curves correspond to different values of x .

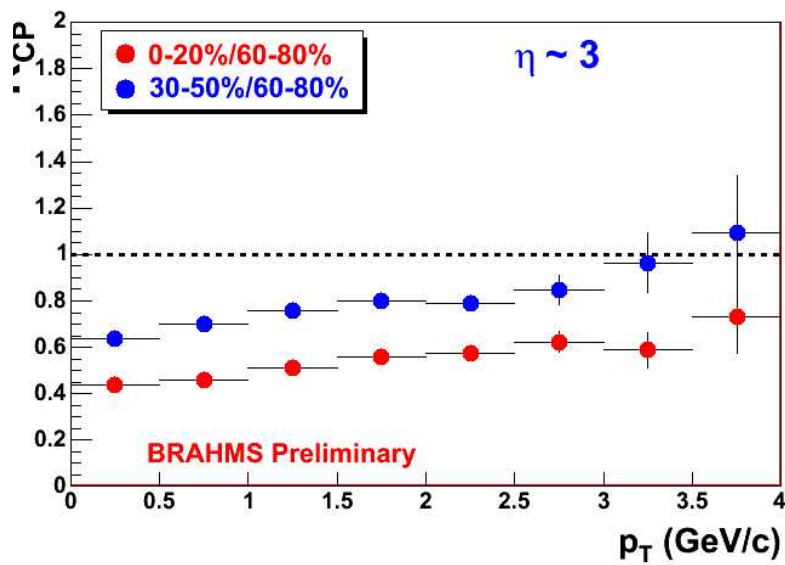


Fig. 32: The measurements from BRAHMS of the ratio of dAu high- p_T particle production to that of incoherent scattering as a function of x and centrality

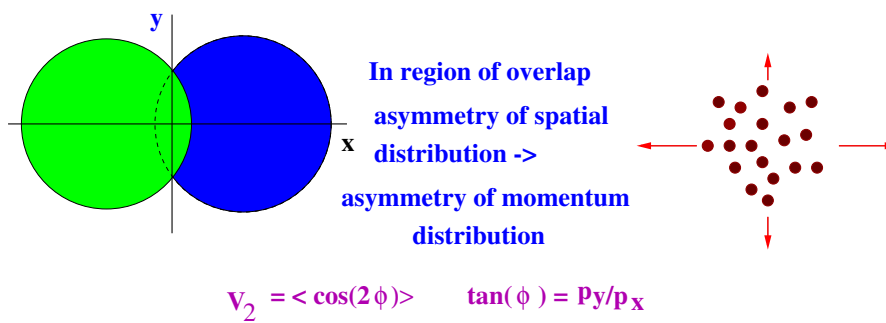


Fig. 33: The asymmetry in the distribution of matter in an off-centre collision is converted to an asymmetry of the momentum space distribution

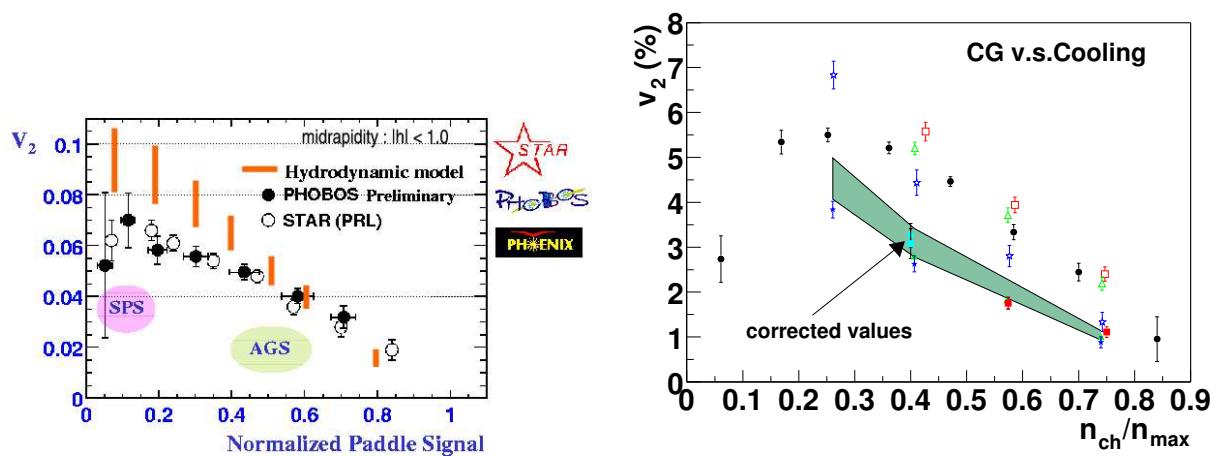


Fig. 34: (a) A hydrodynamic fit to v_2 . (b) The coloured glass fit.

4.6 How strongly does the quark–gluon plasma interact?

4.6.1 Jets are quenched

One of the most interesting results from the RHIC experiments is the so-called ‘jet quenching’ [15], [42–45]. In Fig. 35(a), the single-particle hadron spectrum is scaled by the same result in pp collisions and scaled by the number of collisions. The number of collisions is the number of nucleon–nucleon interactions, which for central collisions should be almost all of the nucleons. One is assuming hard scattering in computing this number, so that a single nucleon can hard-scatter a number of times as it penetrates the other nucleus. The striking feature of this plot is that the ratio does not approach one at large p_T . This would be the value if these particles arose from hard scattering which produced jets of quarks and gluons, and the jets subsequently decayed.

The explanation for this is shown in Fig. 35(b). Here a pair of jets is produced in a gluon–gluon collision. The jets are immersed in a quark–gluon plasma, and rescatter as they poke through the plasma. This shifts the transverse-momentum spectrum down, and the ratio to pp collisions, where there is no significant surrounding media, is reduced.

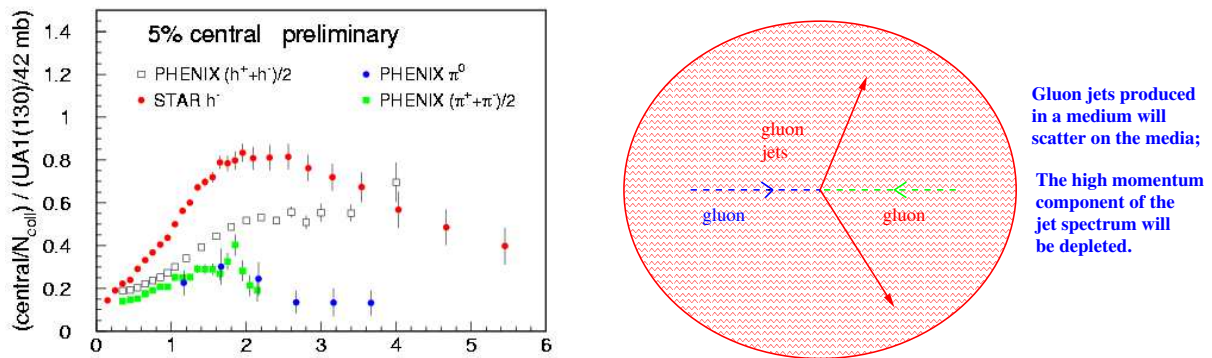


Fig. 35: (a) The p_T distribution of particles scaled by the data from pp collisions times the number of hard collisions inside the nuclei. (b) A pair of jets is produced in a hard collision and they propagate through the surrounding matter.

This suppression has been conclusively shown to be a final-state effect. One can measure the corresponding suppression in dA collisions, and at the central rapidity values where one sees strong suppression in jet production in AuAu collisions, there is little suppression or even enhancement seen in dA collisions. One can also look at the correlation in azimuthal angle of high- p_T -produced particles, as shown in Fig. 36. In pp collisions, if there is a high- p_T particle produced, then at an azimuthal angle 180 degrees away, one expects to see an excess of hard particles. This was done and verified in STAR. In central AuAu collisions, one looks in the backward direction, and the peak has disappeared.

The essential problem with jet quenching is that it is much stronger than expected from naive QCD computation. Jet quenching apparently persists out to 20 GeV. For charmed particles, the observed jet quenching defies realistic QCD computations.

One of the reasons why jet quenching is so important for the RHIC programme is that it gives a good measure of the degree of thermalization in the collisions. If jets are strongly quenched by transverse momenta of 4 GeV, then because cross-sections go like $1/E^2$ for quarks and gluons, this would be strong evidence for thermalization at the lower energies typical of the emitted particles.

4.6.2 The matter flows and is well approximated by perfect fluid hydrodynamics

One can look for evidence of thermalization directly from the measured p_T distributions. Here one can do a hydrodynamic computation and in so far as it agrees with the results, one is encouraged to believe that there is thermalization. On the other hand, these distributions may have their origin in the

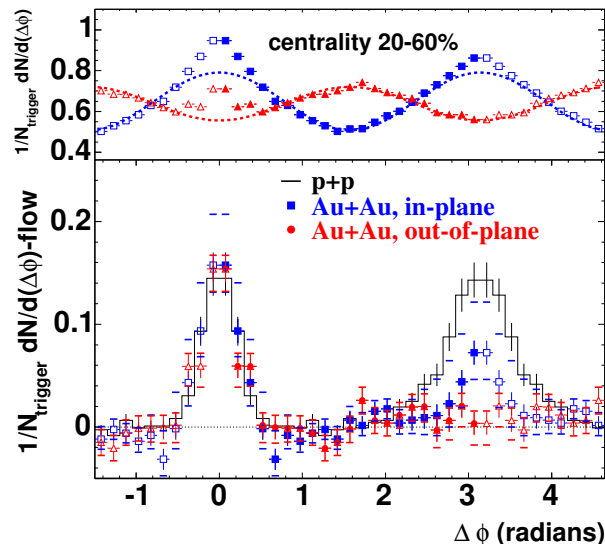


Fig. 36: The forward-backward correlation for high- p_T particles produced in STAR

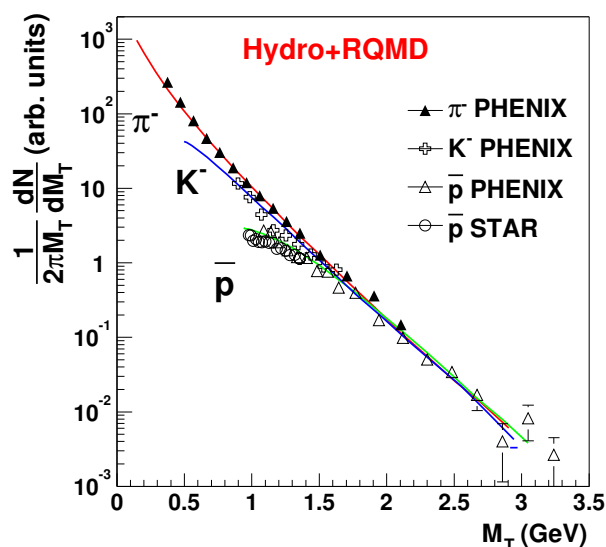


Fig. 37: The hydrodynamical model fits to the m_T spectra for the PHENIX and STAR data

initial conditions for the collision, the coloured glass. In reality, one will have to understand the tradeoff between both effects. The hydrodynamic models do a good job in describing the data for $p_T \leq 2$ GeV. Here there is approximate m_T scaling, a characteristic feature of hydrodynamic computations. This scaling arises naturally because hydrodynamic distributions are produced by flowing matter which has a characteristic transverse flow velocity with a well-defined local temperature. Particles with the same m_T should have arisen from regions with the same transverse-flow velocity and temperature.

Hydrodynamical models successfully describe the data on m_T distributions [46]. In Fig. 37 the results of the simulation by Shuryak and Teaney are shown compared to the STAR and PHENIX data [15]. The shape of the curve is a prediction of the hydrodynamic model, and is parametrized somewhat by the nature of the equation of state. Notice that the STAR data include protons near threshold, and here the m_T scaling breaks down. The hydrodynamic fits get this dependence correctly, and this is one of the best tests of this description. The hydrodynamic models do less well on fits to the more peripheral collisions. In general, a good place to test the hydrodynamic models' predictions is with massive particles close to

threshold, since here one deviates in a computable way from the m_T scaling curve, which is arguably determined from parametrizing the equation of state.

If one can successfully argue that there is thermalization in the RHIC collisions, then the hydrodynamic computations become compelling. One should remember that hydrodynamics requires an equation of state plus initial conditions, and these initial conditions are determined by coloured glass. Presumably, a correct description will require the inclusion of both types of effects [47].

At present, hydrodynamical models do an excellent job of describing data on distributions of particles with $p_T \leq 2$ GeV. This uses perfect fluid hydrodynamics with no viscosity. This was not the case at CERN [48]. Estimates of the viscosity which is consistent with the experimental data give numbers which are quite small, leading some to conclude that the quark–gluon plasma is the most perfect fluid yet measured. There are of course some uncertainties in these conclusions, largely associated with the initial conditions for the hydrodynamic equations, uncertainty in the equation of state, and dispersion in the treatment of the matter at late times when the hydrodynamic description must break down. Nevertheless, the fact that the hydrodynamic computations seem to work well, and the existence of strong jet quenching, lead me to conclude that at a minimum, the matter produced is reasonably well approximated as a thermal system, and is remarkably strongly self-interacting. This means that I believe that the semi-quantitative conclusions drawn from hydrodynamic simulation have substance.

4.7 Confinement and chiral symmetry restoration

We would like to know whether or not deconfinement has occurred in dense matter or whether chiral symmetry restoration has changed particle masses.

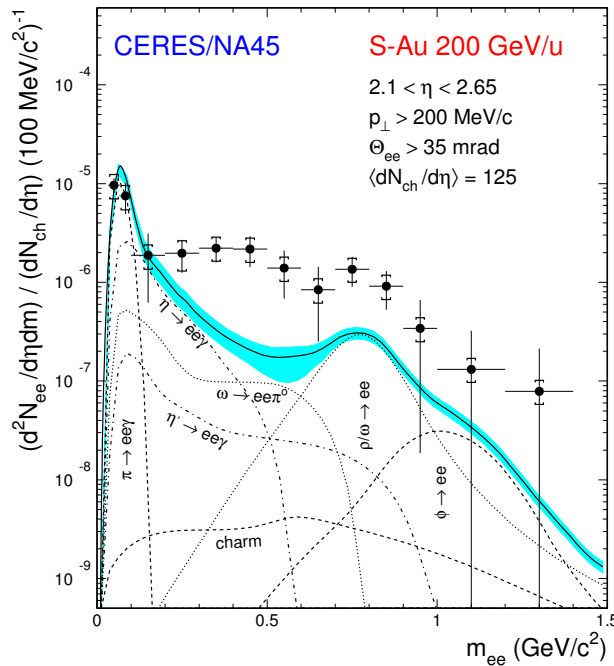


Fig. 38: The CERES data on low-mass electron–positron pairs. The expected contribution from ordinary hadrons is shown by the solid line. The data points are for the measured electron–positron pairs.

This can be studied in principle by measuring the spectrum of dileptons emitted from the heavy-ion collision. These particles probe the interior of the hot matter since electromagnetically interacting particles are not significantly attenuated by the hadronic matter. For electron–positron pairs, the mass distribution has been measured in the CERES experiment at CERN [49], and is shown in Fig. 38. Shown

in the plot is the distribution predicted from extrapolating from pA collisions. There should be a clear ρ and ϕ peak, which has disappeared. This has been interpreted as a resonance mass shift [50], enhanced η' production [51], but is most probably collisional broadening of the resonances in the matter produced in the collisions [52]. Nevertheless, if one makes a plot such as this and the energy density is very high and there are no resonances at all, then this would be strong evidence that the matter is not hadronic, i.e., the hadrons have melted.

The resolution in the CERES experiment is unpleasantly large, making it difficult to unambiguously interpret the result. Whether or not such an experiment could be successfully run at RHIC, much less whether the resolution could be improved, is the subject of much internal debate among the RHIC experimentalists.

It has also been pointed out recently that the matter in the early stages after the collisions has remarkable properties [13]. At the earliest times, there is both longitudinal colour electric and colour magnetic fields. These fields evolve towards a thermalized system as the longitudinal fields evaporate into gluons. I call this early matter the glasma. The fields have a non-zero colour $\vec{E} \cdot \vec{B}$. This is an unusual situation and generates an anomaly in the axial vector current. This means that even very energetic quarks will flip their helicities in the presence of such fields, and generate chiral symmetry breaking. It has been conjectured that such helicity flip may ultimately be responsible for mass generation in QCD. The idea of the glasma with its anomalous fields is recent, and it is not yet possible to assess the experimental implications.

4.8 Confinement and J/Ψ suppression

The NA(50) data for J/Ψ production is shown in Fig. 39 [53]. In the first figure, the ratio of J/Ψ production cross-section to that of Drell–Yan is shown as a function of E_T , the transverse energy, for the lead–lead collisions at CERN. There is a clear suppression at large E_T which is greater than the hadronic

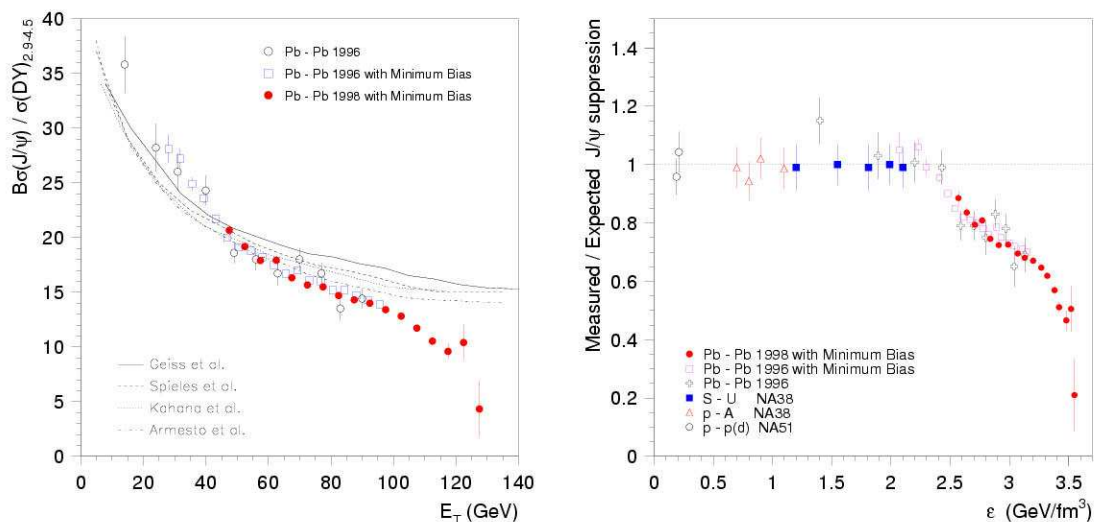


Fig. 39: (a) The ratio of produced J/Ψ pairs to Drell–Yan pairs as a function of transverse energy E_T at CERN energy. (b) The measured compared to the theoretically expected J/Ψ suppression as a function of the Bjorken energy density for various targets and projectiles.

absorption model calculations which are plotted with the data [54]. In the next figure, the theoretically expected J/Ψ suppression based on hadronic absorption models is compared to that measured as a function of the Bjorken energy density for various targets and projectiles. There appears to be a sharp increase in the amount of suppression for central lead–lead collisions.

Is this suppression due to Debye screening of the confinement potential in a high-density quark–gluon plasma [55–57]. Might it be due to higher twists, enhanced rescattering, or changes in the gluon distribution function [58, 59]. Might the J/ψ suppression be changed into an enhancement at RHIC energies and result from the recombination in the produced charm particles, many more of which are produced at RHIC energy [60–63].

These various descriptions can be tested by using the capability at RHIC to do pp and pA as well as AA collisions. Issues related to multiple scattering, higher twist effects, and changes in the gluon distribution function can be explored. A direct measurement of open charm will be important if final-state recombination of the produced open charm makes a significant amount of J/ψ 's.

The data from the PHENIX experiment show roughly the same pattern of suppression as seen at CERN [64]. This is a surprise since one naively expected that there should be more suppression at higher energy densities. This had led some to speculate that there may be significant recombination effects in the final state [60], [63]. This will be resolved after measurements of resonant states decaying into charm, J/ψ flow, and more, as the programme at RHIC continues.

4.8.1 Direct photons

One of the first suggestions for a signal of the quark–gluon plasma was thermal radiation due to photons [65–69]. Produced photons are penetrating, and in principle can measure the properties of the hot matter at early times in the collision. The problem is that there are huge backgrounds from resonance decays.

At very large p_T , the resonance backgrounds are small, but there the dominant process for making photons is hard scattering of a gluon and a quark, and reflects the initial parton distribution functions. This has been measured at RHIC, and agrees with perturbative computations. More recently, there has been a claimed measurement from PHENIX of an excess seen at intermediate p_T [70].

The excess is surely interesting, but it is an excess relative to a theoretical computation, and these computations must be checked against the pp and dA data before one can be too excited about the result seen in AA. Of course, one has to check against all possible sources of photons for AA before one concludes that these photons arise from thermal radiation. As the results are new, these checks are not yet complete.

4.8.2 The lifetime and size of the matter produced

The measurement of correlated pion pairs, the so-called HBT pion interferometry, can measure properties of the space–time volume from which the hadronic matter emerges in heavy-ion collisions [71]. The quantities R_{long} , R_{side} and R_{out} shown in Fig. 40 measure the transverse size of the matter at decoupling and the decoupling time.

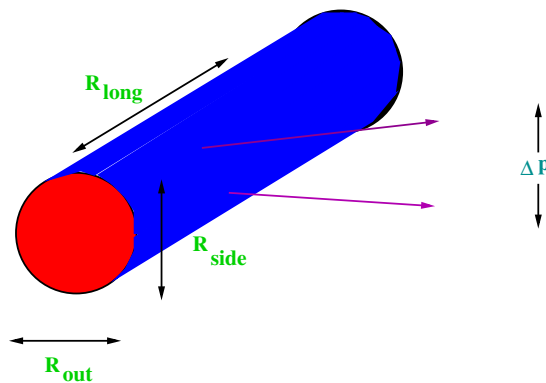


Fig. 40: The various radii used for HBT pion interferometry

In Fig. 41, the data from STAR and PHENIX are shown [15]. There is only a weak dependence on energy, and the results seem to be more or less what was observed at CERN energies. This is a surprise, since a longer time for decoupling is expected at RHIC. Perhaps the most surprising result is that $R_{\text{out}}/R_{\text{side}}$ is close to 1, whereas most theoretical expectations give a value of about $R_{\text{out}}/R_{\text{side}} \sim 2$ [72, 73]. Perhaps this is due to greater than expected opacity of the emitting matter? At this time, there is no consistent theoretical description of the HBT data at RHIC. Is there something missing in our space–time picture?

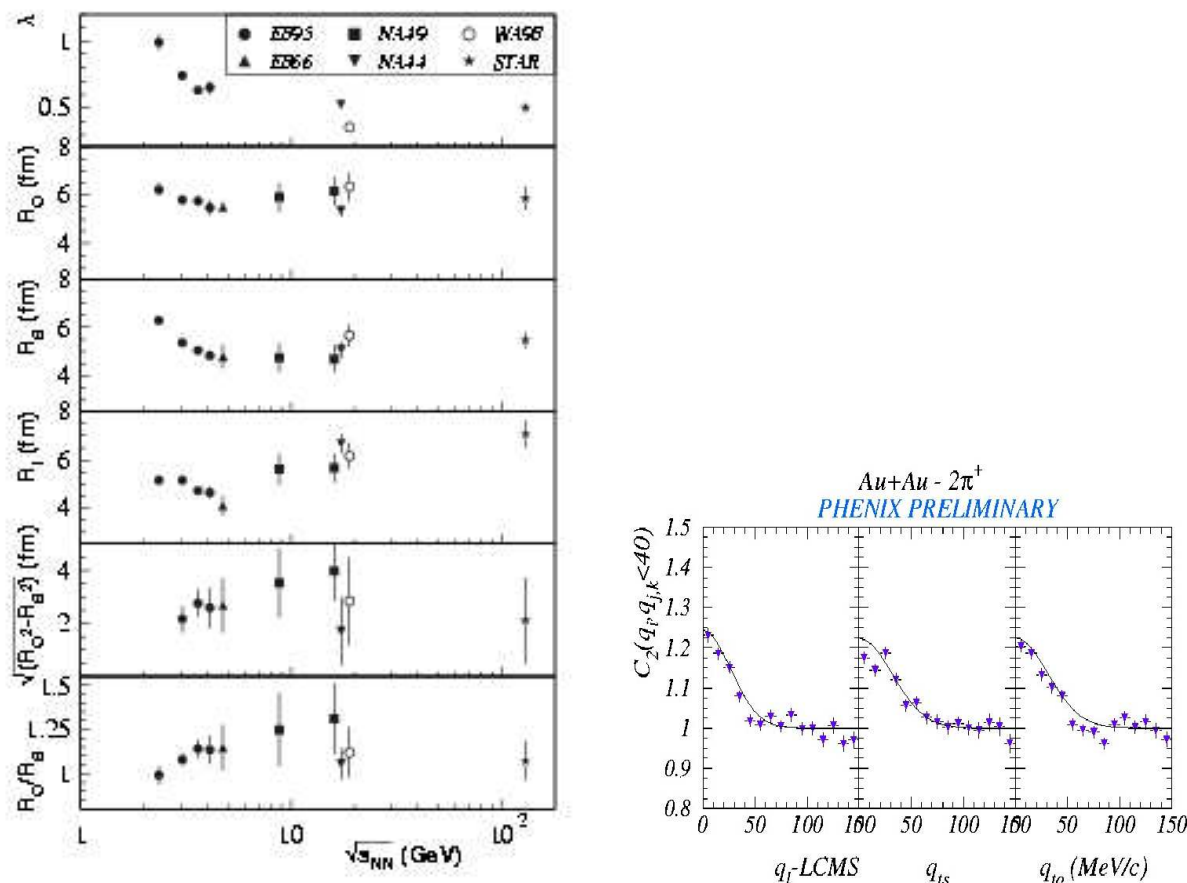


Fig. 41: (a) The various HBT radii measured in heavy-ion experiments including the new data from STAR. (b) The correlation functions which determine the radii as a function of the pair momenta measured in PHENIX.

4.8.3 The flavour composition of the quark–gluon plasma

The first signal proposed for the existence of a quark–gluon plasma in heavy-ion collisions was enhanced strangeness production [74]. This has led to a comprehensive programme in heavy-ion collisions to measure

the ratios of abundances of various flavours of particles [75]. In Fig. 42(a), the ratios of flavour abundances are compared to a thermal model for the particle abundances [76–78]. The fit is quite good. In Fig. 42(b), the temperature and baryon chemical potential extracted from these fits is shown for experiments at various energies and with various types of nuclei. It seems to agree reasonably well with what might be expected for a phase boundary between hadronic matter and a quark–gluon plasma.

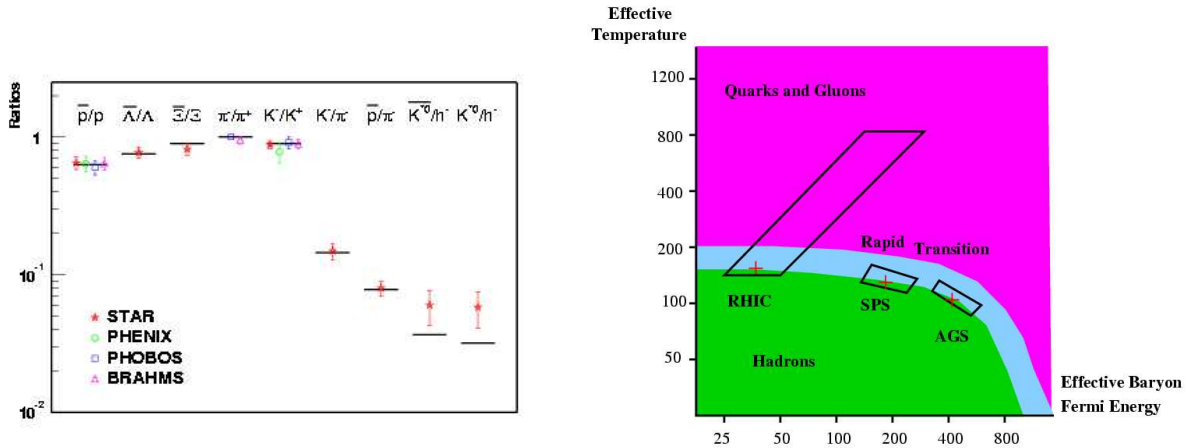


Fig. 42: (a) Various ratios of particle abundances and the RHIC data. The lines are the predictions of a thermal model. (b) The temperature vs baryon chemical potential for a thermal model which is fit to data at various energies. The dashed line is a hypothetical phase boundary between a quark–gluon plasma and a hadronic gas.

This would appear to be a compelling case for the production of a quark–gluon plasma. The problem is that the fits done for heavy ions to particle abundances work even better in $e^+ e^-$ collisions. One definitely expects no quark–gluon plasma in $e^+ e^-$ collisions. There is a deep theoretical question to be understood here: How can thermal models work so well for non-thermal systems? Is there some simple saturation of phase space? The thermal model description can eventually be made compelling for heavy-ion collisions once the degree of thermalization in these collisions is understood.

Acknowledgements

I gratefully acknowledge conversations with Dima Kharzeev, Robert Pisarski and Raju Venugopalan on the subject of this talk.

This manuscript has been authorized under Contract No. DE-AC02-98H10886 with the U.S. Department of Energy.

References

- [1] For a summary of recent results, see the excellent review talk by Jean-Paul Blaizot, Lectures at the 40th Internationale Universitätswochen für Kern- und Teilchenphysik: Ddense Matter (IUKT 40), Schladming, Styria, Austria, 2001, Lectures on Quark Matter, L. Mathelitsch and W. Plessas [Eds.], Lect. Notes Phys. **583** (2002) 117–160, [hep-ph/0107131].
- [2] For a state-of-the-art, up-to-date review on the properties of the colour glass condensate, see E. Iancu and R. Venugopalan, in Quark–Gluon Plasma 3, W. N. Wang and R. C. Hwa [Eds.] (World Scientific, Singapore, 2004), [hep-ph/0303204].
- [3] For a review about the prospects for spin physics at RHIC and other accelerators, see G. Bunce, N. Saito, J. Soffer and W. Vogelsang, *Annu. Rev. Nucl. Part. Sci.*, **50** (2000) 525.
- [4] J. C. Collins and M. J. Perry, *Phys. Rev. Lett.* **34** (1975) 1353.
- [5] For a summary of recent results, see the excellent review talk by F. Karsch, Lectures at the 40th Internationale Universitätswochen für Kern- und Teilchenphysik: Ddense Matter (IUKT 40), Schladming, Styria, Austria, 2001, Lectures on Quark Matter, L. Mathelitsch and W. Plessas [Eds.], Lect. Notes Phys. **583** (2002) 209–249, [hep-lat/0106019].

- [6] L. V. Gribov, E. M. Levin and M. G. Ryskin, *Phys. Rep.* **100** (1983) 1; A. H. Mueller and Jianwei Qiu, *Nucl. Phys.* **B268** (1986) 427; J.-P. Blaizot and A. H. Mueller, *Nucl. Phys.* **B289** (1987) 847; L. D. McLerran and R. Venugopalan, *Phys. Rev.* **D49** (1994) 2233; **D49** (1994) 3352; E. Iancu, A. Leonidov and L. D. McLerran, *Nucl. Phys.* **A692** (2001) 583; E. Ferreiro, E. Iancu, A. Leonidov and L. D. McLerran, hep-ph/0109115.
- [7] J. Breitweg *et al.*, *Eur. Phys. J.* **67** (1999) 609.
- [8] M. Froissart, *Phys. Rev.* **123** (1961) 1053.
- [9] A. Martin, *Nuovo Cim.* **42** (1966) 930; L. Lukaszuk and A. Martin, *Nuovo Cim.* **52** (1967) 122.
- [10] E. Ferreiro, E. Iancu, K. Itakura and L. McLerran, *Nucl. Phys.* **A710** (2002) 373.
- [11] A. Kovner and U. Wiedemann, *Phys. Rev.* **D66** (2002) 051502; *Phys. Lett.* **B551** (2203) 311.
- [12] A. Kovner, L. D. McLerran and H. Weigert, *Phys. Rev.* **D52** (1995) 6231; **D52** (1995) 3809; A. Krasnitz and R. Venugopalan, *Phys. Rev. Lett.* **84** (2000) 4309; *Nucl. Phys.* **B557** (1999) 237; A. Krasnitz, Y. Nara and R. Venugopalan, *Phys. Rev. Lett.* **87** (2001) 192302.
- [13] T. Lappi and L. McLerran, *Nucl. Phys.* **A772** (2006) 200 [hep-ph/0602189].
- [14] S. Mroczynski, *Phys. Lett.* **B214** (1988) 587; **B314** (1933) 118; **B363** (1997) 26; P. Arnold, J. Lenaghan and G. Moore, *JHEP* **0308** (2003) 002; P. Arnold, J. Lenaghan, G. Moore and L. Yaffe, *Phys. Rev. Lett.* **94** (2005) 072302; P. Romatschke and M. Strikland, *Phys. Rev.* **D68** (2003) 036004; **D70** (2004) 116006; P. Romatschke and R. Venugopalan, *Phys. Rev. Lett.* **96** (2006) 062302; A. Dumitru and Y. Nara, *JHEP* **0509** (2005) 041; A. Dumitru, Y. Nara and M. Strikland, *Phys. Lett.* **B621** (2005) 89.
- [15] See the Whitepapers published by the BRAHMS, PHENIX, PHOBOS and STAR experiments for the original data and references. *Nucl. Phys.* **A757** (2005) 1; *Nucl. Phys.* **A757** (2005) 27; *Nucl. Phys.* **A757** (2005) 102; *Nucl. Phys.* **A757** (2005) 184.
- [16] J. Jalilian-Marian, A. Kovner, L. McLerran and H. Weigert, *Phys. Rev.* **D55** (1997) 5414.
- [17] J. Jalilian-Marian, A. Kovner, A. Leonidov and H. Weigert, *Nucl. Phys.* **B504** (1997) 415; *Phys. Rev.* **D59** (1999) 014014.
- [18] R. Baier, A. H. Mueller, D. Schiff and D.T. Son, *Phys. Lett.* **B502** (2001) 51.
- [19] D. Kharzeev and M. Nardi, *Phys. Lett.* **B507** (2001) 121.
- [20] M. Gyulassy and Xin-Nian Wang, *Comput. Phys. Commun.* **83** (1994) 307.
- [21] K. Eskola, K. Kajantie, P. Ruuskanen and K. Tuominen, *Nucl. Phys.* **B570** (2000) 379; K. Eskola, K. Kajantie and K. Tuominen, *Phys. Lett.* **B497** (2001) 39.
- [22] D. Kharzeev and E. Levin, nucl-th/0108006.
- [23] L. McLerran, 12th International Workshop on Deep Inelastic Scattering, Štrbské Pleso, Slovakia, 2004, D. Bruncko, J. Ferencei and P. Strizenec [Eds.] (Slovak Acad. Sci. Inst. Exp. Phys., Kosice, 2004), p. 161.
- [24] K. Golec-Biernat and M. Wustoff, *Phys. Rev.* **D60** (1999) 114023.
- [25] A. M. Staśto, K. Golec-Biernat and J. Kwieciński, *Phys. Rev. Lett.* **86** (2001) 596.
- [26] E. Iancu, K. Itakura and L. McLerran, *Nucl. Phys.* **A708** (2002) 327.
- [27] E. Iancu, K. Itakura and S. Munier, *Phys. Lett.* **B590** (2004) 199.
- [28] A. H. Mueller and D. Triantafyllopoulos, *Nucl. Phys.* **B640** (2002) 331; D. Triantafyllopoulos, *Nucl. Phys.* **B648** (2003) 294.
- [29] D. Kharzeev, E. Levin and L. McLerran, *Phys. Lett.* **B561** (2003) 93.
- [30] J. Jalilian-Marian, Y. Nara and R. Venugopalan, *Phys. Lett.* **B577** (2003) 54.
- [31] D. Kharzeev, Y. Kovchegov and K. Tuchin, *Phys. Rev.* **D68** (2003) 094013.
- [32] R. Baier, A. Kovner and U. Wiedemann, *Phys. Rev.* **D68** (2003) 054009; J. Albacete, N. Armesto, C. Salgado and U. Wiedemann, *Phys. Rev. Lett.* **92** (2004) 082001.

- [33] Jian-Wei Qiu and I. Vitev, *Phys. Lett.* **B632** (2006) 507.
- [34] E. Iancu, K. Itakura and D. Triantafyllopoulos, *Nucl. Phys.* **A742** (2004) 182.
- [35] I. Vitev, *Phys. Lett.* **B562** (2003) 36.
- [36] A. Dumitru, A. Hayashigata and J. Jalilian-Marian, *Nucl. Phys.* **A765** (2006) 464.
- [37] S. Voloshin and Y. Zhang, *Z. Phys.* **C70** (1996) 665; A. M. Poskhanzer and S. A. Voloshin, *Phys. Rev.* **C58** (1998) 1671; J. Y. Ollitrault, *Phys. Rev.* **D46** (1992) 229.
- [38] P. F. Kolb, J. Sollfrank and U. Heinz, *Phys. Lett.* **B459** (1999) 667; P. F. Kolb, P. Huovinen, U. Heinz and H. Heiselberg, *Phys. Lett.* **B500** (2001) 232.
- [39] A. Krasnitz, Y. Nara and R. Venugopalan, *Phys. Lett.* **B554** (2003) 21.
- [40] J. Adams *et al.*, *Phys. Rev. Lett.* **94** (2005) 062301.
- [41] S. Adler *et al.*, *Phys. Rev. Lett.* **94** (2005) 082301; K. Adcox *et al.*, *Phys. Rev. Lett.* **88** (2002) 192303.
- [42] J. D. Bjorken, FERMILAB-PUB-82-059-THY.
- [43] D. Appel, *Phys. Rev.* **D33** (1986) 717.
- [44] J. P. Blaizot and L. McLerran, *Phys. Rev.* **D34** (1986) 2739.
- [45] M. Gyulassy, P. Levai and I. Vitev, *Nucl. Phys.* **B571** (2000) 197; *Phys. Rev. Lett.* **85** (2000) 5535; *Nucl. Phys.* **B594** (2001) 371.
- [46] D. Teaney and E. V. Shuryak, *Phys. Rev. Lett.* **83** (1999) 4951; D. Teaney, J. Lauret and E. V. Shuryak, nucl-th/0110037.
- [47] D. K. Srivastava, *Phys. Rev.* **C64** (2001) 064901.
- [48] M. Gyulassy and L. McLerran, *Nucl. Phys.* **A750** (2005) 30.
- [49] G. Agakishiev *et al.*, *Nucl. Phys.* **A638** (1998) 159.
- [50] G. E. Brown and M. Rho, *Phys. Rep.* **269** (1996) 333.
- [51] J. Kapusta, D. Kharzeev and L. D. McLerran, *Phys. Rev.* **D53** (1996) 5028.
- [52] R. Rapp, G. Chanfray and J. Wambach, *Phys. Rev. Lett.* **76** (1996) 368.
- [53] For the latest results, see M. C. Abreau *et al.*, in 14th International Conference on Ultra-Relativistic Nucleus–Nucleus Collisions, Quark Matter, Turin, Italy, 1999, *Nucl. Phys.* **A661** (1999) 93.
- [54] J. Geiss, E. Bratkovskaya, W. Cassing and C. Greiner, Presented at Workshop on Charmonium Production in Relativistic Nuclear Collisions, Seattle, WA, 1998 [nucl-th/9810059]; C. Speies, R. Vogt, L. Gerland, S. A. Bass, M. Bleicher, H. Stocker and W. Greiner, *Phys. Rev.* **C60** (1999) 054901; D. E. Kahana and S. H. Kahana, *Phys. Rev.* **C60** (1999) 065206; N. Armesto, A. Capella, E. Ferreira, A. Kaidalov and D. Sousa, *Nucl. Phys.* **A698** (2002) 583.
- [55] T. Matsui and H. Satz, *Phys. Lett.* **B178** (1986) 416.
- [56] D. Kharzeev and H. Satz, *Phys. Lett.* **B334** (1994) 155.
- [57] J.-P. Blaizot and J.-Y. Ollitrault, *Phys. Rev. Lett.* **77** (1996) 1703.
- [58] J. Armesto and A. Capella, *Phys. Lett.* **B430** (1998) 23; A. Capella, E. G. Ferreira and A. Kaidalov, *Phys. Rev. Lett.* **85** (2000) 2080.
- [59] Jian-wei Qiu, J. P. Vary and Xiao-fei Zhang, hep-ph/9809442.
- [60] R. Thews, M. Schroedter and J. Rafelski, *Phys. Rev.* **C63** (2001) 054905.
- [61] P. Braun-Munzinger and J. Stachel, *Phys. Lett.* **B490** (2000) 196.
- [62] P. Braun-Munzinger and K. Redlich, *Eur. Phys. J.* **C16** (2000) 519.
- [63] M. Gazdzicki and M. Gorenstein, *Phys. Rev. Lett.* **83** (1999) 4009; M. Gorenstein, A. P. Kostyuk, H. Stoecker and W. Greiner, *Phys. Lett.* **B509** (2001) 277; M. Gorenstein, A. Kostyuk, L. McLerran, H. Stoecker and W. Greiner, hep-ph/0012292; M. Gorenstein, A. Kostyuk, H. Stocker and W. Greiner, *Phys. Lett.* **B524** (2002) 265.

- [64] S. Adler *et al.*, *Phys. Rev.* **C69** (2004) 014901.
- [65] E. Shuryak, *Phys. Lett.* **B78** (1978) 150.
- [66] K. Kajantie and H. I. Miettinen, *Z. Phys.* **C9** (1981) 341.
- [67] D. Srivastava and B. Sinha, 11th International Conference on Ultra-Relativistic Nucleus–Nucleus Collisions, Quark Matter 1995, Monterey, CA, 1995, *Phys. Rev. Lett.* **73** (1994) 2421.
- [68] E. L. Feinberg, *Nuovo Cim.* **A34** (1976) 391.
- [69] L. McLerran and T. Toimela, *Phys. Rev.* **D31** (1985) 545.
- [70] S. Adler *et al.*, *Phys. Rev. Lett.* **94** (2005) 232301, see also the proceedings of 18th International Conference on Ultra-Relativistic Nucleus–Nucleus Collisions, Quark Matter 2005, Budapest, Hungary (2005).
- [71] M. Gyulassy, S. Kauffmann and L. Wilson, *Phys. Rev.* **C20** (1979) 2267.
- [72] S. Chapman, P. Scotto and U. Heinz, *Phys. Rev. Lett.* **74** (1995) 4400; S. Chapman and U. Heinz, *Phys. Lett* **B340** (1994) 250.
- [73] S. Soff, S. Bass and A. Dumitru, *Phys. Rev. Lett.* **86** (2001) 3981.
- [74] B. Muller and J. Rafelski, *Phys. Rev. Lett.* **48** (1986) 1066; P. Koch, B. Muller and J. Rafelski, *Phys. Rep.* **142** (1986) 167.
- [75] For a summary, see M. Kaneta and N. Xu, in 5th International Conference on Strangeness in Quark Matter, Strangeness 2000, Berkeley, CA, 2000, *J. Phys.* **G27** (2001) 589.
- [76] For a state-of-the-art assessment review, see J. Cleymans, *Pramana J. Phys.* **60** (2003) 787 [hep-ph/0201142]; J. Cleymans and K. Redlich, *Phys. Rev. Lett.* **81** (1998) 5284; *Phys. Rev.* **C60** (1999) 054908.
- [77] P. Braun-Munzinger, J. Stachel, J. P. Wessels and N. Xu, *Phys. Lett.* **B365** (1996) 1; P. Braun-Munzinger, I. Heppe and J. Stachel, *Phys. Lett.* **B465** (1999) 15.
- [78] G. Yen and M. Gorenstein, *Phys. Rev.* **C59** (1999) 2788.